High-Resolution Helium Atom Time-of-Flight Spectroscopy of Low-Frequency Vibrations of Adsorbates

Frank Hofmann and J. Peter Toennies*

Max Planck Institut für Strömungsforschung, Bunsenstrasse 10, 37073 Göttingen, Germany

Received November 1, 1995 (Revised Manuscript Received January 4, 1996)

Contents

I. Introduction

The atomic-level description of the interatomic interactions determining the structure and dynamics of clean and adsorbate-covered surfaces is one of the most fundamental topics in surface science. It enters as a prerequisite in any attempt to understand the important processes of adsorption and desorption, catalytic reactions, friction and lubrication, epitaxial growth and related phenomena on a microscopic scale. Of particular interest is the bonding character of the adsorbed molecules with the substrate, the interaction between adsorbed species, as well as the influence of the substrate on the chemical bonds within the adsorbed molecules. Also the adsorption-induced modifications of the substrate structure and electronic properties are of fundamental importance.

One of the most direct approaches to gain information on adsorbate−substrate interactions is the spectroscopy of vibrational modes of the adsorbed molecules. The maximum number of vibrational modes of an adsorbed molecule amounts to $3N$, where N is the number of atoms within the molecule. Of the $3N$ normal modes $3N - 6$ modes are characterized by vibrational amplitudes localized within the adsorbed molecule ("internal modes"), and the remaining six modes correspond to frustrated vibrations and rotations of the whole adsorbed molecule ("external modes" or "librational modes") with respect to the surface.

Spectroscopy of the internal modes supplies information on the influence of the substrate on the intramolecular chemical bonds. From the frequencies of these vibrations the type and strength of the bond between single atoms of the adsorption system can be derived. The identification of molecules by using their vibrational spectra as a "fingerprint" is a standard procedure in surface chemical analysis.

The external modes are more directly sensitive to the interaction of the entire molecule with the substrate. Since for the external vibrations the effective mass involved in the vibrations is considerably larger than in the case of the localized intramolecular vibrations, and the binding energies are usually less than the chemical bonds within the molecule, the corresponding energies of the external modes are generally much smaller than the energies of the internal modes. It should be noted, however, that for large molecules the situation is more complicated, since also low-energetic internal torsional and deformation modes are expected. The external modes are rather strongly affected by adsorbate−adsorbate interactions much more so than the internal modes. In this review we will focus mainly on the external substrate−adsorbate and adsorbate−adsorbate interactions, where the adsorbed molecule can be essentially regarded as a rigid object.

The vibrational energies of the external modes are directly related to the potential energy surface of the molecule bound to the surface. The adsorption potential can be coarsely characterized by the adsorption energy E_{ad}, which determines the vibrations polarized perpendicular to the surface, and by the diffusion barrier E_D characterizing the lateral variation of the adsorption energy. Since the diffusion barrier amounts only to a small fraction of the adsorption energy ($E_D/E_{ad} \approx 0.02-0.3$),[1−3] the vibrational modes associated with in-plane displacements show generally considerably lower vibrational frequencies than the modes polarized perpendicular to the surface.

As an example, in Figure 1a the structure of one of the simplest adsorbate systems is shown, a single CO molecule adsorbed at an on-top site of a fcc(001) metal surface. For CO on metal substrates generally a perpendicular adsorption geometry is found, with the carbon atom closer to the surface. For the normal coordinates[4,5] shown in Figure 1b all the corresponding vibrational energies have been determined by inelastic electron scattering (EELS), infrared spectroscopy (IRS), and helium atom scattering (HAS). The internal C−O stretch mode ($\hbar\nu(\omega_1) = 257.8$ meV)[6] has by far the highest energy. The remaining three modes are external modes, with a 2-fold degeneracy

S0009-2665(95)00220-2 CCC: $25.00

Frank Hofmann was born in 1964 in Tübingen. After studying physics in Stuttgart he completed his "Diplom" thesis in 1989 under the supervision of Professor J. P. Toennies at the Max-Planck-Institut für Strömungsforschung in Göttingen. Here he was involved in experimental studies of the lattice dynamics of layered crystals using the helium atom scattering (HAS) technique. In the period between 1991 and 1995 he built a new and improved HAS apparatus at the same Institut and completed his Ph.D. with detailed studies of the dynamics of clean and adsorbate-covered metal surfaces. Since January 1996 he has been employed as a system planner at Mercedes-Benz AG in Sindelfingen, Germany.

Professor Peter Toennies is director of the research group Molecular Interactions in the "Max Planck Institut für Strömungsforschung" in Göttingen. He was born and educated in the United States where he received his Ph.D. in physical chemistry at Brown University in 1957. He then moved to Bonn, Germany, to carry out the first molecular beam state-to-state scattering experiments with Hans Bennewitz in the University Physics Institute of Professor Wolfgang Paul. He was awarded the Venia Legendi (habilitation) at the University of Bonn in 1965. In 1969 he accepted his presentation position as a director and scientific member of the Max-Planck-Society. In 1971 he became an adjunct professor at the Universities of Göttingen and Bonn. He is a corresponding member of the Academy of Sciences in Göttingen and a member of the "Deutsche Akademie der Natuforscher Leopoldina" in Halle. He has received a number of scientific awards such as the Physics Prize of the Göttingen Academy of Sciences (1964), the Gold Heyrovsky Medal of the Czechovlovak Academy of Sciences (1991), the Hewlett-Packard Europhysics Prize in Condenser Matter Research (1992), and the Max-Planck Prize with Giorgio Benedek (1992). He is married and has two daughters.

of the frustrated rotations ν_3 and of the frustrated translations ν_4. Below the CO desorption temperature of $T_{des}\approx160$ K ($kT_{des}\approx14$ meV), both the C−Cu stretch mode ($\hbar\omega(\nu_2) = 42.8$ meV)[6] and the frustrated rotation ($\hbar\omega(\nu_3) = 35.3$ meV)[7] are hardly populated and might therefore also be classified as "high-energy modes". Therefore, for CO on Cu(001) only the frustrated translational mode parallel to the surface with its extremely low energy of ($\hbar\omega(\nu_4) = 3.94$ meV)[8] can be thermally excited. Since the ν_4 mode invariably has the lowest energy and, moreover, is most important for understanding surface molecular dynamics, it will play a central role in the present review. Here we will refer to the C−Cu stretch mode ν_2 and the frustrated translational mode ν_4 as the S- and T-modes, respectively.

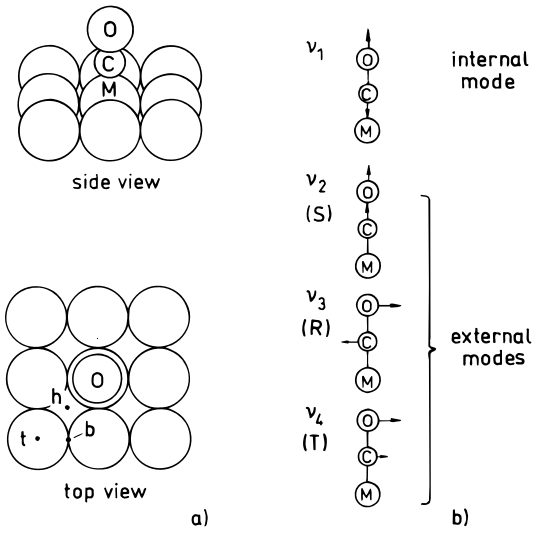

Figure 1. The structure (a) and vibrational modes (b) of CO adsorbed on an on-top site on a fcc(001) surface. The four fundamental modes are the C−O stretch mode (ν_1), the C−metal stretch mode (ν_2), the frustrated rotation (ν_3), and the frustrated translation parallel to the surface (ν_4). In the top view in a the location of the different possible high symmetry surface sites, on-top (t), bridge (b), and hollow (h), are indicated.

The interactions between adsorbed molecules are expected to be influenced by the substrate.[11] In the case of physisorption systems it is often assumed that the effective adsorbate−adsorbate interactions are similar to the corresponding gas-phase interactions, although some modifications even in these simple cases are expected. Generally the physisorbed atoms aquire a small, static dipole moment due to exchange-correlation interactions of the adsorbate's valence electrons and the substrate's electrons, leading to a small additional repulsive contribution to the lateral potential.[12,13] On metal substrates also the ubiquitous van der Waals attractive interaction between the physisorbed molecules can be enhanced due to image dipole effects.[14]

In the chemisorption of atoms and molecules on metallic surfaces the situation is considerably more complicated, since a very large charge transfer between the metal and the adsorbate often occurs, resulting in a strong repulsive dipole-dipole interaction. The highly polarizable metal substrate also reacts on the dipoles by forming the well known Friedel oscillations in the surface electron density, which surround the bonding site,[15−17] and by an elastic deformation of the substrate lattice,[18−21] leading to further indirect contributions to the lateral adsorbate−adsorbate interactions. Moreover, for adsorption systems involving a significant charge transfer between the adsorbate and the substrate the Fermi surface of the substrate can be modified substantially, leading to a completely modified surface chemistry.[15] At the present time the quantitative prediction of these subtle effects is beyond the capabilities of first principles calculations.[22]

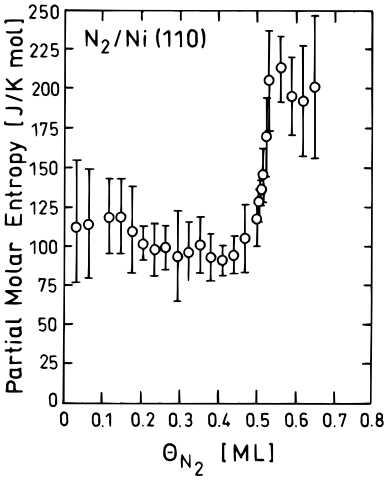

Figure 2. Partial molar entropy $\tilde{S}_{ad}$ of N_2 adsorbed on Ni(110) as a function of coverage.[24] The entropy values have been obtained from adsorption isobars at a surface temperature $T_S \approx 150$ *K*. The entropy is practically exclusively determined by the lateral translational degrees of freedom. The sharp rise at $\Theta = 0.5$ ML is attributed to density fluctuations within the adsorbed layer due to the formation of domain walls at coverages $\Theta > 0.5$ ML.[24]

The balance between adsorbate−adsorbate and adsorbate−substrate interactions is of major relevance for a wide range of chemical and physical adsorbate properties. For example, it determines the very rich manifold of ordered structures and structural phase transitions observed for most adsorption systems.[23] A comprehensive survey on the theoretical aspects of adsorbate structure and phase transitions can be found in the recent review by Persson.[23] Obviously these properties depend not only on the potential energy surface, but also on the entropic contributions to the adsorbate free energy that has to be minimized in a stable arrangement. In this context the librational modes are again of relevance, since these modes due to their very low energies are easily thermally occupied and contribute predominantly to the adsorbate entropy. A particularly well-documented example for this relationship is the chemisorption system N_2/Ni(110), where the partial molar entropy of the adsorbed layer has been measured as a function of the coverage.[24] As shown in Figure 2, the partial molar entropy $\tilde{S}_{ad}$ varies between 100 and 200 J K^{-1} mol^{-1} at a surface temperature of $T_S = 150$ K. The contribution from the perpendicular Ni−N_2 mode ($\hbar\omega = 40$ meV)[25] and from the internal N−N mode ($\hbar\omega = 272$ meV)[25] amounts to only $\tilde{S}_{vib} = 1.4$ J K^{-1} mol^{-1} [24] indicating that the dominant contribution comes from the low-energy librational modes and from the lateral adsorbate diffusion.

Striking examples for the consequences of these entropy effects have been found recently for CO/Ni(001)[26,27] and CO/Pt(111).[28] In both cases the CO molecules can be adsorbed on on-top sites and on bridge sites. Since on bridge sites the CO molecules have only one "easy" direction for the frustrated translational mode,[5] but a 2-fold degeneracy on the on-top sites, the occupancy of the on-top site is entropically favored with increasing temperature. For example by simply varying the surface temperature the on-top site occupation probability P_{top} for CO/Ni(001) can be varied between $P_{top} \approx 20\%$ at $T_S = 70$ K and $P_{top} \approx 65\%$ at room temperature.[26,27]

The shallowness of the lateral adsorption potential and the resulting low vibrational energies of librational modes also have important implications for structural determinations of adsorbed molecules. Various structure-sensitive techniques like extended X-ray absorption fine structure (EXAFS), near-edge X-ray absorption fine structure (NEXAFS), low-energy electron diffraction (LEED), electron-stimulated ion angular distribution (ESDIAD), or X-ray photoelectron diffraction (XPD) obtain a lateral spatial resolution of 0.1 Å or better. For a wide class of adsorption systems this resolution is even at liquid nitrogen temperatures significantly higher than the mean lateral displacement of the adsorbed molecules due to the thermal excitation of librational modes. Therefore, in high-resolution structural analysis the thermal excitations of the librational modes have to be taken explicitly into account.[29] The mean-square displacement of adsorbates as derived from such high-resolution structural analyses is closely related to the corresponding vibrational energy. It has been shown recently that in favorite cases the T-mode energy of adsorbates can be derived with an accuracy of about 1 meV from measurements of the temperature dependence of LEED diffraction intensities.[30]

Since the internal vibrational modes of adsorbed molecules often depend significantly on their lateral position, it is not surprising that these internal adsorbate vibrations are strongly affected by the excitation of low-energy librational modes.[31] Experimentally these well-known vibrational coupling mechanisms show up as temperature-dependent vibrational peak shift and broadening effects ("dephasing").

Accurate experimental information on these low-energy librations has only recently become available. The first measurement of a frustrated translational mode was performed in 1986 by Lahee, Toennies, and Wöll[32] using inelastic helium atom scattering (HAS). Since then most of the quantitative information on these modes has been obtained so far almost exclusively by the HAS technique. Recently the more established spectroscopic techniques have also contributed experimental information in this area. The most important properties of these techniques are compared in Table 1.

The bulk dynamical properties of solid and liquid materials have been investigated with great success by inelastic neutron scattering (INS) with the introduction of high flux neutron reactors in the 1950s.[33] With this technique a good energy resolution and wavevector transfers over the full relevant range up to several $Å^{-1}$ can be obtained. In addition, the scattering interaction is rather simple, and INS spectra can be interpreted even when applied to rather complicated materials.[34] Surface investigations, however, are seriously hampered by the extremely small scattering cross sections. Even in the more favorable case of hydrogen a total cross section σ of only $\sigma \approx 82$ barn (1 barn $= 10^{-8}$ $Å^2$) is found.[33] Therefore, single-crystal surface investigations are essentially not accessible to this technique. To overcome this problem powders or other polycrystalline materials with a large effective surface area have

Table 1. Comparison of Commonly Used Surface Vibrational Spectroscopy Techniques

technique	spectral range (meV)	resolution (meV)	momentum transfer	sensitivity (monolayers)]
inelastic neutron scattering (INS)	$\lesssim 100$	$>10^{-2}$	average over BZ	≥ 1
infrared spectroscopy (IRS)	$\gtrsim 22$	0.1	≈ 0	$>10^{-3}$
inelastic electron scattering (EELS)	$\gtrsim 5$	>1 typically: ≈ 4	variable	$>10^{-4}$
helium atom scattering (HAS)	$0.2-\approx 50$	>0.08 typically: 0.3	variable	$>10^{-3}$

been used as substrates.[34] The results are then an average over a distribution of different microscopic surfaces and molecular orientations. In this way, a number of spectroscopic results on the internal and external modes of larger adsorbed molecules have been obtained.[34,35]

Infrared spectroscopy (IRS) has a high inherent resolution for modes with vibrational energies $\hbar\omega$ in the range from about 22 to 300 meV.[7,36] Even with the newly available synchroton light sources the very low-energetic frustrated translational modes with typical vibrational energies $\hbar\omega < 10$ meV are not accessible to this technique. In addition dipole selection rules apply which strongly reduce the number of observable modes. In particular, since the frustrated translational and rotational modes are largely polarized parallel to the surface they are in principle dipole forbidden. Recently, however, it has been shown that in favorable cases these modes can give rise to an antiabsorption resonance, which has been detected by infrared reflectivity measurements.[7,37,38] IRS is restricted to negligibly small wavevectors.

With inelastic electron scattering (EELS) some of the limitations encountered with IRS are circumvented. In the dipole sensitive mode at incident kinetic energies of several electronvolts only limited information on the wavevector dependence is available but an energy resolution of 1 meV can be obtained.[39] However, in the high-resolution mode the EELS sensitivity is dramatically reduced.[39] In the impact region at incident energies of 50−200 eV the dispersion curves can be measured over the full Brillouin zone with an energy resolution of several millielectronvolts.[39] Only a rather small number of successful applications of this technique to spectroscopy of low-energy librational modes has been reported so far (see section IV). This situation may change with the development of improved EELS spectrometers, which have recently become available.[39] High-resolution EELS is largely restricted to conducting surfaces and radiation damage may affect weakly bound systems.[40]

The HAS technique has the unique advantage of perfect surface sensitivity and complete absence of any destructive side effects even on the most sensitive physisorption systems. Moreover it provides information on the entire dispersion curves. Since it does not depend on surface conductivity it can be applied equally well to insulators, semiconductors, and metals. In addition it accesses lower energies not accessible to other techniques. Also the microscopic details of the dynamics of adsorbate diffusion has recently become accessible.[41,42]

In the present article we review recent developments in the rich field of adsorbate dynamics, with particular emphasis on the results obtained by helium atom scattering. In this respect it can be regarded as a continuation of the recent, comprehensive review of Benedek and Toennies of the dynamics of clean surfaces.[43] In the next experimental section (section II) the experimental apparatus and procedures are described. In section III selected experimental results are discussed. On the basis of a comparative analysis of the large available experimental data base, in section IV an attempt is made to find general trends and relations between the lateral adsorbate interactions and other adsorption parameters. Finally we conclude in section V and discuss some future trends.

II. Experimental Methods

A. He Atom Scattering Apparatus

A schematic diagram of a typical helium atom scattering apparatus similar to the ones in use in our laboratory in Göttingen is shown in Figure 3. The He beam is produced by expanding He gas at a pressure of typically 30 up to 200 bar through an aperture of about 10 μm in diameter into vacuum.[44,45] This produces an intense beam of atoms with a velocity spread of $\Delta v/v \lesssim 1\%$. The most probable beam velocity v can be varied from 3000 m/s ($\approx$120 meV, $k_i = 16$ Å^{-1}, $\lambda_{dB} = 0.3$ Å, where λ_{dB} is the de Broglie wave length) down to $\approx$700 m/s ($\approx$8 meV, $k_i = 4$ Å^{-1}, $\lambda_{dB} = 1.5$ Å) by simply changing the temperature of the source from 300 to 40 K, respectively. For this range of incident beam energies the energy half-width lies between about 1 and 0.2 meV. For inelastic time-of-flight (TOF) measurements the beam is mechanically chopped by a rotating disc multislit chopper, and the TOF distributions are measured by a multichannel scaler.

After passing through the skimmer and three differential pumping stages the helium beam is directed at the crystal surface, which is contained in a differentially pumped ultrahigh vacuum chamber with a base pressure in the low 10^{-11} mbar range. Usually the scattering chamber contains conventional crystal cleaning (ion sputter gun) and analyzing devices such as low-energy electron diffraction (LEED) and an Auger spectrometer.

The scattered He atoms are detected using a mass spectrometer with an electron bombardment ionizer which is optimized for high sensitivity. In order to reduce the helium background in the detector resulting from the large helium gas flux into the target chamber, a number (3−4) of additional differential pumping stages is placed between the scattering chamber and the detector. In this way, with altogether nine differential pumping stages between the source and detector chambers the He partial

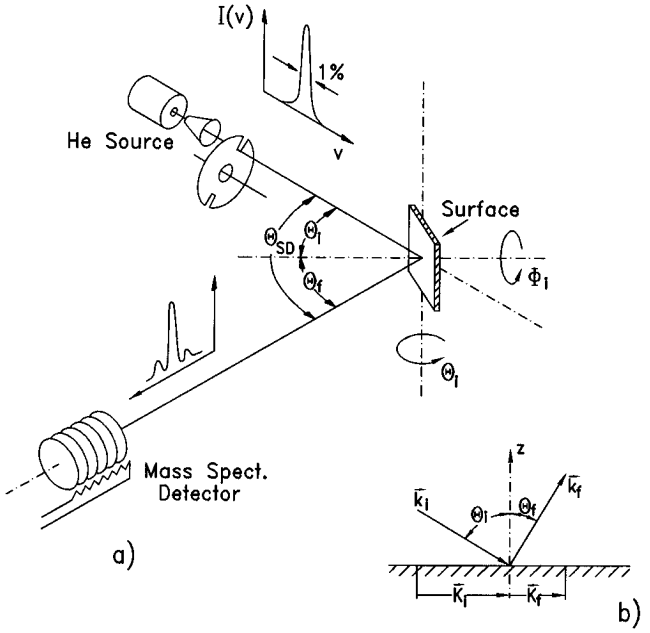

Figure 3. (a) Schematic view of the apparatus and a typical velocity distribution of the incident beam and of the scattered beam in a helium atom scattering experiment. For ease of construction, in most existing high-resolution HAS spectrometers a fixed-angle scattering geometry is used (θ_{SD} = const). Then by rotating the target the angular distribution of the scattered intensity can be measured. For inelastic scattering studies the incident beam is pulsed by passing it through a rotating chopper disk and measuring the time-of-flight distribution of the scattered He atoms. (b) The scattering kinematics are completely defined by the incident (index i) and final (index f) wavevectors k and scattering angles θ. The surface plane components of the wavevector are denoted by K_i and K_f.

pressure in the detector is reduced to 10^{-15} mbar ($\approx$ 10 He atoms/cm^3). This corresponds to a background He ion count rate of less than 10 counts/s compared to an incident beam signal which is about 10^8-10^9 counts/s. For ease of construction, in most existing high-resolution HAS spectrometers a fixed angle scattering geometry is used (θ_{SD} = const). The scattering kinematics are then determined by the incident energy E_i and the incident scattering angle θ_i.

The frequencies ω and wavevector transfers $\Delta\mathbf{K}$ of the adsorbate vibrations involved can be determined from the measured energy change $\hbar\omega$ and scattering angles via the conservation equations:

$$\hbar\omega = \frac{\hbar^2}{2m}(k_i^2 - k_f^2) \quad (1)$$

$$\Delta\mathbf{K} = k_f \sin\theta_f - k_i \sin\theta_i \quad (2)$$

where k_i and k_f are the initial and final wavevectors of the probe particle with mass m and θ_i and θ_f are the incident and final scattering angles, respectively (see Figure 3). Note that negative (positive) values of $\hbar\omega$ correspond to the creation (annihilation) of a vibrational quantum. Equations 1 and 2 show that by simply varying the incident kinematical conditions (E_i and θ_i), the full ($\hbar\omega$, $\Delta\mathbf{K}$) space can be mapped out. In the wavevector coordinate $\Delta\mathbf{K}$, generally the full Brillouin zone can be mapped out and energy transfers up to 30−50 meV are accessible.

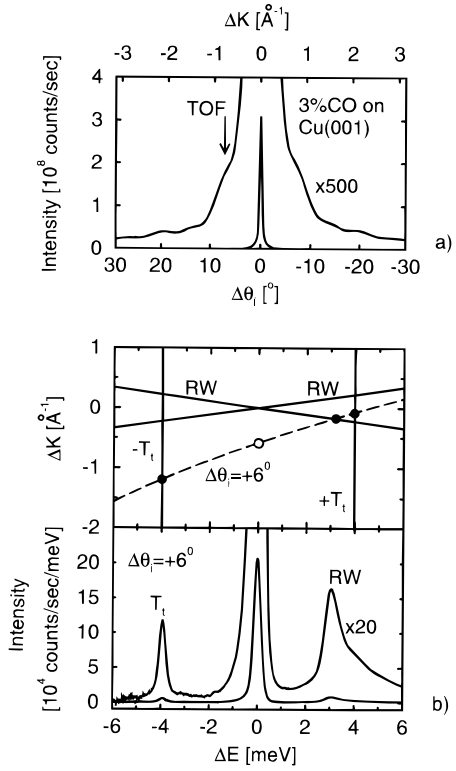

Figure 4. (a) Typical angular distribution of helium atoms scattered from a small coverage of 3%CO on Cu(001)[48] at an incident energy of E_i = 11 meV, and a surface temperature of T_S = 50 K. The top abscissa indicates the corresponding parallel wavevector transfer while the bottom abscissa indicates angular increments away from the specular peak at θ_i = 47.8°. The weak intensity undulations are due to diffraction from the randomly distributed isolated CO molecules.[52] (b) The lower panel shows a time-of-flight spectrum taken at an incident angle of θ_i = 53.9°. The corresponding scan curve (dashed line) as well as the dispersion curves of the substrate Rayleigh mode (RW) and of the adsorbate T-mode (T_t) are also shown (upper panel). The inelastic peak at $\Delta E \approx +3.5$ meV is attributed to the annihilation of a single quantum of the substrate Rayleigh wave (RW) phonons. The other inelastic peak at −4 meV (T_t) is due to the creation of an on-top T-mode quantum. Under these experimental conditions the scattering is dominated by elastic scattering and small inelastic contributions due to single substrate phonons and adsorbate vibrations.

In order to illustrate the two major types of HAS measurements, Figure 4 shows a typical angular distribution and a time-of-flight spectrum of He atoms scattered from a 3% coverage of CO molecules adsorbed on a Cu(001) surface. The angular distribution in a shows an extremely strong specular peak at $\Delta\theta = 0°$, which originates from the large uncovered area of the copper surface. The 500× magnified curve shows a small additional intensity contribution, which decreases rapidly at large values of $|\Delta\theta|$. The TOF spectrum in b taken at $\Delta\theta = +6°$ shows that the latter intensity contribution originates predominantly from He atoms scattered elastically from the adsorbed CO molecules. In addition, the TOF spectrum shows an inelastic peak at $\Delta E \approx -4$ meV which is attributed to the creation of a T-mode quantum. The other large inelastic peak, which happens to be at +3.5 meV, is due to the annihilation of a single substrate Rayleigh wave phonon quantum.

The full characterization of the adsorbate dynamics requires in addition to their vibrational dispersion curves a determination of the corresponding vibrational polarization vectors. With spectroscopic tools, this problem is often approached by a careful analysis of the scattered intensities. For HAS the scattering theory has been completely worked out both for periodic surfaces[49] and for isolated adsorbate molecules.[50] To a good approximation the measured differential reflection coefficient $d^3R/dE_f\, d\Omega_f$, which is proportional to the number of scattered particles detected per unit final solid angle and per unit final energy, can be written as a product of a form factor $|\tau_{if}|^2$ and a dynamical structure factor $S(\Delta\mathbf{K}, \omega)$:[50]

$$\frac{d^3R}{d\Omega_f\, dE_f} = \frac{1}{(2\pi)^2\hbar^4}\frac{m^2 k_f}{|k_{iz}|}|\tau_{if}|^2 S(\Delta\mathbf{K},\omega) \qquad (3)$$

where m is the mass of an He atom and k_{iz} is the perpendicular component of the incident wavevector. The form factor $|\tau_{if}|^2$ accounts for the microscopic scattering mechanism of the He atom with the adsorbate molecule and is completely defined by the shape of the scattering potential and the scattering dynamics. For flat surfaces the form factor is strongly peaked toward $\Delta K = 0$, whereas for corrugated surfaces or isolated adsorbates the form factor becomes spread over a larger angle range.[50] Different approximate expressions for the form factor can be found in ref 50.

Of more direct relevance in the context of vibrational spectroscopy is the dynamical structure factor $S(\Delta\mathbf{K}, \omega)$, which describes both the dynamics and the structure of the surface. The structure factor $S(\Delta\mathbf{K},\omega)$ has been derived both for ordered surfaces[50] and for isolated adsorbates.[52] For single-phonon scattering, by neglecting diffraction effects and assuming an in-plane scattering geometry, it can be expressed as

$$S(\Delta\mathbf{K},\omega) = |\Delta k_z^2\epsilon_z^2 + \Delta\mathbf{K}^2\epsilon_l^2|\frac{n^{\pm}(\hbar\omega)}{\omega}\, e^{-2W} \qquad (4)$$

where $n^{\pm}(\hbar\omega)$ denotes the Bose factor for excitation and annihilation of one vibrational quantum, $\exp(-2W)$ is the Debye−Waller factor, Δk_z and ΔK are the perpendicular and parallel components of the wavevector transfer Δk and ϵ_z,ϵ_l are the perpendicular and longitudinal components of the vibrational polarization vector ϵ. Within the Einstein approximation of the adsorbate dynamics (noninteracting oscillators with mass M and frequency ω), the Debye−Waller exponent can by expressed as:[47]

$$2W = \frac{\hbar}{M\omega}(\Delta\mathbf{k}\epsilon)^2[n(\omega) + {}^1/_2] \qquad (5)$$

For a less simplistic treatment of the Debye−Waller factor the reader is referred to ref 51. By using the relation that the Debye−Waller exponent $2W$ amounts approximately to the average number of vibrational quanta transferred by the scattering process,[50] the condition for predominantly single-phonon scattering is $2W \lesssim 1$.

From eq 4 the following propensity rules concerning the effect of polarization vectors in the scattering intensities of adsorbate vibrational modes can be formulated: (1) With the usual in-plane scattering geometry where the plane defined by $\boldsymbol{k}_i$ and $\boldsymbol{k}_f$ passes through the surface normal Z, vibrations with an out-of-plane polarization cannot be excited. (2) Longitudinally polarized modes cannot be excited at $\Delta K = 0$ and their transition probabilities increase with ΔK. It should be noted that this latter rule is only approximately obeyed in real systems since surface vibrations are generally elliptically polarized.[43] Additional complications arise since He atoms are sensitive to the small electron density (10^{-3}−10^{-5} atomic units) at about 3 Å above the surface layer of atoms. It has been shown recently that in the case of metallic surfaces the electron density does not always follow the ion core motion.[43] (3) In typical HAS experiments with a backscattering geometry (e.g. $\theta_i+\theta_f \approx 90°$) the perpendicular wavevector transfer Δk_z depends only weakly on the scattering angles and is always much larger than the parallel wavevector transfer ΔK. Therefore perpendicularly polarized modes are generally detected with the highest sensitivity. Consequently the wavevector dependence of perpendicularly polarized modes is dominated by the scattering form factor, which has a pronounced maximum at $\Delta K = 0$.

III. Selected Results

In this section the type of information that can be obtained by HAS is illustrated using a few representative examples. Three related areas of increasing complexity are considered sequentially. The easiest access to adsorbate−substrate interactions is obtained by investigating the low-frequency external librational modes and diffusion of isolated adsorbate molecules, which are considered first in section III.A. The influence of adsorbate−adsorbate interactions is described in the following section III.B. Finally in section III.C we describe some recent applications of the HAS technique to more complex systems.

A. Adsorbate–Substrate Interactions

1. Lateral Potentials

At very low adsorbate coverages it is possible to investigate adsorbate−substrate interactions without the additional complication of adsorbate−adsorbate interactions. This condition may, however, be difficult to realize for certain adsorbates. For example, physisorbed rare gases are known to usually form islands even at low coverages.[53] Other adsorption systems, like alkali metals, adsorbed on metal surfaces exhibit extremely long-ranged repulsive interactions, which even at coverages as low as 5% of a monolayer lead to significant lateral structural and vibrational correlations (see section B.2). For many chemisorbed species on metals however, randomly spaced, practically uncorrelated low coverage adsorption systems can be readily prepared. Examples are the adsorption of CO on the low-index metal surfaces of copper[54] and nickel[55] which are described next.

A series of typical time-of-flight spectra, converted to an energy-transfer scale, of He atoms scattered from a Cu(001) surface covered with a 3% monolayer

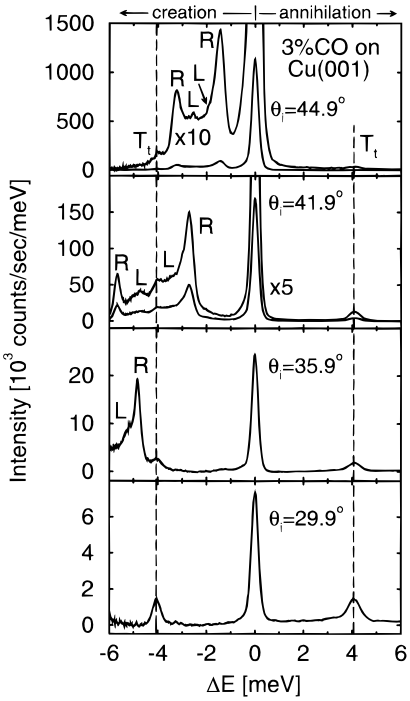

Figure 5. A series of typical He atom scattering inelastic time-of-flight spectra converted to an energy-transfer scale taken at different incident angles θ_i (compare with Figure 4b). The low-energy frustrated translational mode (T_t) of a 3% monolayer coverage of CO molecules on a Cu(001) surface at on-top sites is seen in both creation and annihilation. In addition several inelastic peaks are seen which can be attributed to the excitation of substrate Rayleigh phonons or of the longitudinal resonance, here denoted by R and L, respectively. The incident energy was $E_i = 11.4$ meV, and the surface temperature was $T_S = 150$ *K*.

of CO is shown for scattering angles smaller than the specular in Figure 5 (compare with Figure 4b).

The spectrum shows in addition to a strong peak at zero energy transfer sharp inelastic peaks both on the creation side ($\Delta E < 0$) and on the annihilation side ($\Delta E > 0$). The dispersive substrate excitations due to the excitation of substrate Rayleigh phonons (RW) and of the longitudinal resonance (LR) are easily identified by their dependence on the incident angle θ_i. We will focus in the following on the frustrated translational mode at the on-top sites (T_t) $\Delta E \approx \pm 4$ meV.

For coverages below 5% of a monolayer the T-mode peak position and shape is independent of the kinematical conditions and of the CO coverage, indicating the absence of any significant adsorbate−adsorbate interactions. Thus the interpretation of these spectra is relatively straightforward since all the observed results can be attributed solely to adsorbate−substrate interactions.

For the same system, the detailed nature of the normal mode displacements involved in the T-mode was recently investigated by measuring the effect of isotopic substitution of the atoms in the CO molecule.[8,48] The results of these measurements are summarized in Figure 6. The graph shows the T-mode energy as a function of surface temperature for the four different isotopomers $^{12}C^{16}O$, $^{12}C^{18}O$, $^{13}C^{16}O$, and $^{13}C^{18}O$. For all isotopes the differences in the T-mode energy of less than 0.025 meV are

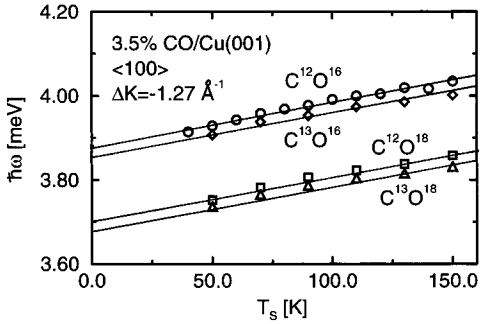

Figure 6. The T-mode frequency of a 3% monolayer coverage of CO on Cu(001) for four different isotopes as a function of the surface temperature.[48] The T-mode energy shows a weak, approximately linear, increase with the surface temperature due to an anharmonic coupling of the CO molecule to the substrate. The very weak dependence on the mass of the carbon atom and the rather strong dependence on the mass of the oxygen atom indicate a significant "tilting" component in the T-mode displacement pattern.

distinctly resolved. The frequencies of all isotopes increase slightly with increasing temperature, indicating a weak anharmonic coupling of the CO molecules with the copper substrate.[56] This effect will be discussed further in section III.A.3. The weak dependence of the T-mode energy on the mass of the carbon atom, which is closest to the surface, compared to the rather strong dependence on the oxygen mass indicate a significant "tilting" displacement of the on-top oxygen atoms with the C-atom remaining nearly stationary. Similar displacement patterns have been derived from model calculations of CO on Al(111)[28] and on Ni(001)[5] and from recent ab initio calculations of CO/Pd(110).[57] At the present time however sufficiently precise ab initio calculations for interpreting the HAS experiments are not yet available. Therefore, empirical potential energy surfaces seem to be the best way to analyze and discuss the lateral dynamics of adsorbed molecules.

Isotope data like those shown in Figure 6 can be used to construct a potential hypersurface as a function of the position of the molecule and its orientation in the vicinity of the equilibrium position at the on-top site.[58] Figure 7 shows a two-dimensional cut in the (x,θ) plane through an empirical multidimensional potential determined recently for CO/Cu(001) along the ⟨110⟩ direction.[58] Here x is the lateral displacement and θ is the tilt angle of the CO molecule with respect to the surface normal. The slope of the "reaction coordinate" for the lateral motion of the CO molecule at the on-top site describes the weak correlation between the tilt angle and the lateral displacements of the center of mass of the molecule. Since the T-mode energies of CO on Ni(001) and on Cu(001) as well as the corresponding substrate lattice constants are almost identical (see Table 3), we expect a very similar lateral potential shape for CO on Ni(001).

2. Adsorbate Diffusion

Complementary information on the potential energy hypersurface can be obtained from diffusion measurements which provide the energetic barriers between adjacent on-top sites. In the past it was

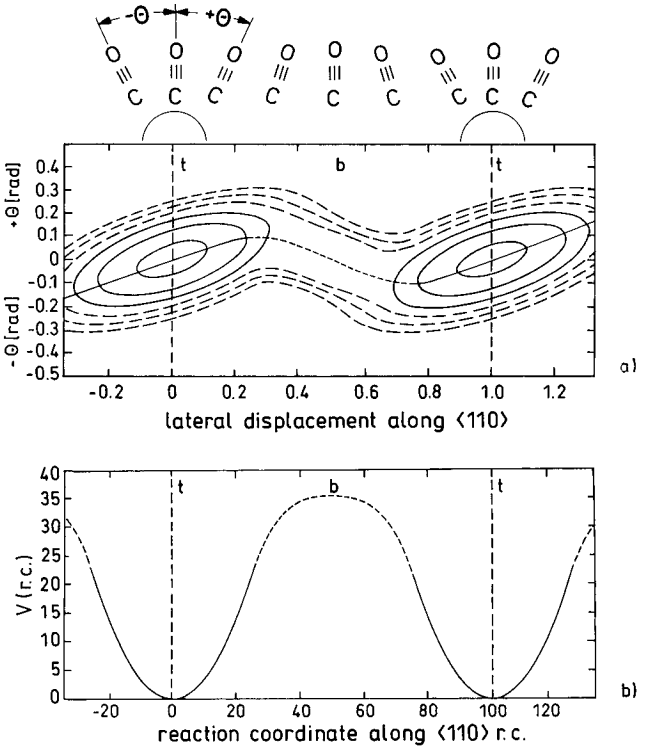

Figure 7. (a) Contour plot of a two-dimensional cut in the (x,θ) plane through an empirically determined multidimensional potential for CO/Cu(001) along the ⟨110⟩ direction.[58] x and θ are the lateral displacement and the tilt angle of the CO molecule with respect to the surface normal, respectively. The equipotential lines have a spacing of 15 meV. The reaction coordinate for the lateral motion of the CO molecule is indicated by the heavy line drawn along the path of minimal potential energy. The corresponding transient CO configurations along the reaction coordinate are shown schematically above. (b) Potential energy along the reaction coordinate along the ⟨110⟩ direction. The shape at the on-top sites are parabolas extrapolated away from these sites. The barrier at the bridge site is derived from QHAS diffusion measurements described in section III.A.2.

found difficult to reconcile the frustrated translational frequencies with the very large experimental barriers for diffusion.[26] For CO on nickel macroscopic measurements of chemical diffusion coefficients yielded diffusion barrier energies of between 95 and 280 meV.[65−68] Recently it has become possible to measure microscopic diffusion coefficients using quasielastic HAS (QHAS). This method has been successfully applied to the diffusion of CO on Ni(001),[59] Ni(110),[3] and Cu(001).[59]

The QHAS technique used in our experiments is entirely analogous to neutron diffraction studies in the bulk.[33] The formal theory goes back to the neutron scattering structure factor calculations of van Hove[61] and has been adapted to the case of helium scattering at surfaces.[42,62] When scattered from diffusing surface atoms the incident wave packet experiences a reduction of its coherence time, leading to a broadening of the scattered energy distribution. This effect is most conveniently observed for the quasielastic peak (see Figure 8) which is attributed to diffuse incoherent elastic scattering from structural defects on the surface. The detailed theoretical analysis revealed that for different microscopic diffusion mechanisms the dynamical structure factor can be expressed as a Lorentzian

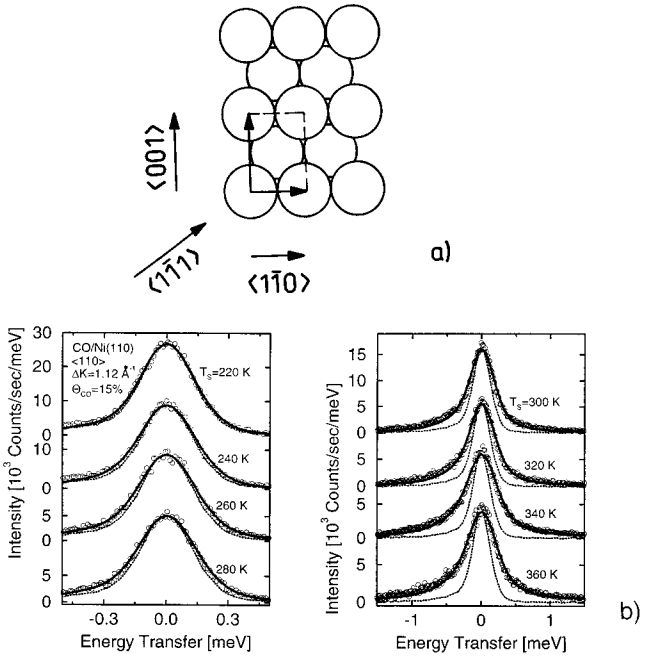

Figure 8. (a) Structure and high-symmetry directions of the fcc(110) surface. (b)Time-of-flight distributions, on an expanded energy transfer scale, of helium atoms scattered along the ⟨1̄10⟩ azimuth from a Ni(110) surface with a low 15% coverage of CO molecules at different surface temperatures $T_S = 220-360$ K.[3] The incident energy is 11.3 meV and the parallel wavevector transfer is $\Delta K = 1.12$ Å^{-1}. The dotted curves (···) are the instrument response function, and the solid lines are a best fit obtained by convoluting the instrument function with a Lorentzian broadening.

$$S(\Delta+\mathbf{K},\omega) = \frac{1}{\pi}\frac{^1/_2\Gamma(\Delta\mathbf{K})}{\{\omega^2 + [^1/_2\Gamma(\Delta\mathbf{K})]^2\}} \qquad (6)$$

where $\Gamma(\Delta\mathbf{K})$ is the energetic broadening of the quasielastic peak as a function of ΔK. The diffusion length l is inversely proportional to ΔK ($l = 2\pi/\Delta K$) and corresponds to distances between ≈2.5 Å ($\Delta K = G$ where G is the reciprocal lattice vector) up to ≈30 Å near the zone origin. Thus the QHAS technique provides information on microscopic diffusion on an atomic length scale. The characteristic diffusion time constant $\tau \approx \hbar/\Gamma_{min}$ corresponding to the smallest resolvable peak broadening of about $\Gamma_{min} \approx 10$ μeV is limited to $\tau \lesssim 65$ ps.

The interpretation of the wavevector dependence of the broadening $\Gamma(\Delta\mathbf{K})$ in terms of a macroscopic diffusion constant requires the knowledge of the microscopic diffusion mechanism. Fortunately, at small wavevector transfers $\Delta K \lesssim 1$ Å^{-1} the quasielastic broadening becomes rather insensitive to the microscopic details of the diffusion mechansim. Therefore, in this region very simple models like the jump model of Chudley and Elliott[63] or the random walk diffusion model lead to rather similar values for the diffusion constants. More sophisticated calculations based on the Mori projection operator formalism[64] or on the results of molecular dynamics simulations[2] have been used to fit the measured $\Gamma(\Delta K)$ curves out to the zone boundary. These theories when applied to the recent QHAS results indicate that diffusion proceeds to a good approximation by fast jumps over the barrier part of the adsorbate−substrate potential,

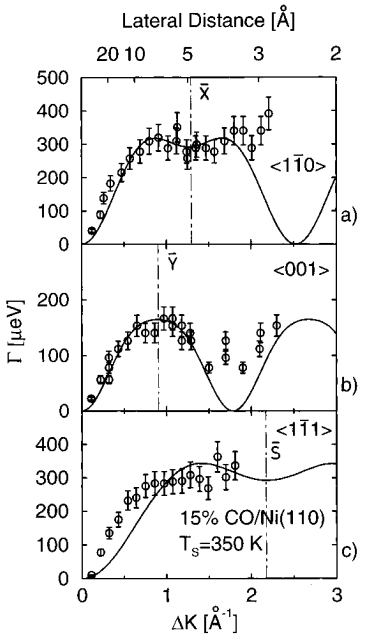

Figure 9. Lorentzian peak width Γ (FWHM) as a function of parallel wavevectors Δ*K* for 15% CO on Ni(110) along three different azimuths.[3] The surface temperature was T_S = 350 *K* and the beam energy E_i = 11.4 meV. The error bars are the standard deviations. The solid line shows the best fit of all the data for a jump model with single and double jumps. The distances corresponding to the Δ*K* values are indicated at the top abscissa.

which are interrupted by long periods where the adsorbate oscillates in the potential wells. Assuming that the vibrational and diffusive motions are completely uncorrelated and that the hopping time is infinitesimally small, the quasielastic broadening can be described to a good approximation within the simple jump model as derived by Chudley and Elliott:[63]

$$\Gamma(\Delta\mathbf{K}) = \hbar\Delta\omega(\Delta\mathbf{K}) = 4\hbar\sum_j \frac{1}{\tau_j}\sin^2\left(\frac{\Delta\mathbf{K}\cdot\mathbf{j}}{2}\right) \qquad (7)$$

where $\boldsymbol{j}$ is the jump vector (j = 1 for a single jump, 2 for a double jump, etc.) and the corresponding jump frequency is $\nu = 1/\tau_j$.

Figure 8 shows a series of time-of-flight spectra featuring the quasielastic peak taken on 10% CO/Ni(110) along the ⟨1$\bar{1}$0⟩ azimuth, which is parallel to the rows of this anisotropic surface.[3] The measurements were performed at an incident beam energy of 11.3 meV with an instrumental resolution of 0.32 meV (FWHM). At low surface temperatures T_S the shape of the quasielastic peak is dominated by the experimental resolution. As T_S is raised above about

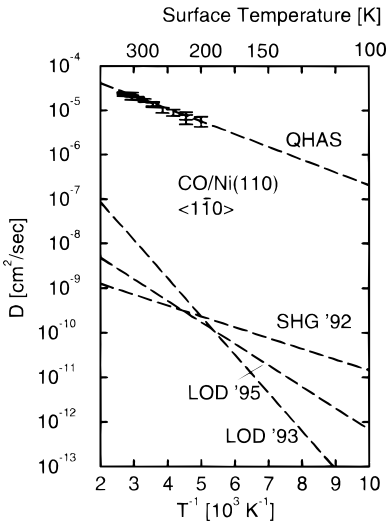

Figure 10. Arrhenius plot of the temperature dependence of the QHAS measured microscopic diffusion coefficients *D* of CO/Ni(110) along the ⟨1$\bar{1}$0⟩ azimuth. For comparison, the results of recent macroscopic diffusion measurements are also shown: SHG'92, ref 69; LOD'93, ref 67; LOD'95, ref 67.

280 K, the quasielastic peak is significantly broadened. To extract the diffusion induced broadening a Lorentzian was convoluted with the instrument function and its width Γ determined by a best fit. Figure 9 shows the dependence of Γ on Δ*K* for three different azimuths on the Ni(110) surface. The solid line shows a best fit for the jump model of eq 7 with single and double jumps. The relative double jump contributions are 38% along the ⟨1$\bar{1}$0⟩ azimuth (parallel to the rows) and 14% along the ⟨001⟩ azimuth. Assuming that diffusion along the ⟨1$\bar{1}$1⟩ azimuth proceeds only via jumps along the ⟨1$\bar{1}$0⟩ and ⟨001⟩ azimuths then these results can be used to calculate the Δ*K* dependence along the ⟨1$\bar{1}$1⟩ azimuth. The reasonably good agreement with the measurements (Figure 9c) provides additional confirmation that the jump model provides a satisfactory description of the data. Therefore, the measured Γ values can be interpreted to a good approximation in terms of a jump diffusion coefficient D_{jump}.

Figure 10 shows the measured temperature dependence of D_{jump} for the case of CO/Ni(001) along the ⟨1$\bar{1}$0⟩ azimuth in the form of an Arrhenius plot. From the slope of the curve the activation barrier E_D and, by extrapolating to $1/T = 0$, the preexponential factor D_0 are determined. The resulting values for this system and other systems studied by the QHAS technique are summarized in Table 2. As seen in Figure 10 the preexponential factors D_0, as determined with QHAS, are orders of magnitude larger

Table 2. Microscopic Adsorbate Activation Barriers and Diffusion Coefficients Determined with QHAS

	coverage (ML)	azimuth	E_D (meV)	D_0 (cm^2/s)	ref
CO/Ni(110)	0.15	⟨1$\bar{1}$0⟩	57 ± 4	(2.1 ± 0.70) × 10^{-4}	3
		⟨001⟩	35 ± 4	(0.7 ± 0.4) × 10^{-4}	
CO/Ni(001)	0.1	⟨100⟩	27 ± 3	(0.5 ± 0.2) × 10^{-4}	59
		⟨110⟩	33 ± 3	(0.7 ± 0.2) × 10^{-4}	
CO/Cu(001)	0.06	⟨100⟩	32 ± 6	≈10^{-5}	59, 118
Na/Cu(001)	0.029	⟨100⟩	53.5 ± 1.4	(0.7 ± 0.3) × 10^{-4}	2, 48
	0.07	⟨1$\bar{1}$0⟩	54 ± 6	(1.8 ± 0.8) × 10^{-4}	48
S/Cu(111)	<0.16	⟨1$\bar{1}$0⟩	–		60
Pb/Pb(110)	self-diffusion	⟨1$\bar{1}$0⟩	650	2.6 × 10^1	41

than the corresponding macroscopic diffusion coefficients measured by the linear optical diffraction (LOD)[67,68] and by the second-harmonic generation (SHG)[69] techniques. Moreover the QHAS activation barriers are smaller by a factor of between 1.7 and 6 compared to the laser experiments. Similar large discrepancies have been found for CO/Ni(100).[59,70] For CO/Cu(001) and Na/Cu(001) a comparison is not possible since measurements of the macroscopic diffusion coefficients have not been published. At present we have no definitive explanation for these large differences. We conjecture that they are due to the much greater influence of surface defects on the macroscopic adsorbate diffusion.[3,59]

The diffusion data shown in Table 2 complement nicely the high resolution HAS measurements of the T-mode frequencies. As evident from Figure 7 for the case of CO/Cu(001), the potential shapes as derived from the isotope dependence of the T-mode is compatible with diffusion barriers of about 35 meV, in excellent agreement with the QHAS results. For the adsorption systems Na/Cu(001),[8,71] CO/Ni(001)[72,59,70] and CO/Ni(110)[3,59] the spectroscopically derived local harmonic potentials valid for small displacements when extended into the anharmonic barrier region are nicely consistent with the measured microscopic QHAS diffusion barriers. Such potential surfaces are an important prerequisite for molecular dynamics simulations[8,73] or diffusion calculations based on the Mori projection operator formalism.[71,83] Another important input is the frictional coupling constant of the molecule to the substrate degrees of freedom. Such measurements have also recently been performed by HAS and are described next.

3. Vibrational Damping

Another important aspect of the lateral adsorbate motion is the influence of possible friction mechanisms. The friction coefficients are key parameters for understanding not only adsorbate diffusion[74] but also the microscopic mechanisms of lubricants.[75] According to theoretical estimates the frustrated translational modes are expected to be strongly damped due to vibrational coupling to the substrate phonons and, in the case of metal substrates, also due to electron−hole pair creation in the substrate.[31,76,77]

Experimentally not much information is available so far. For molecular adsorbates like CO on metal surfaces, the most detailed data on the vibrational damping constants has been extracted from recent laser experiments on CO/Cu(001),[78] CO/Cu(111),[79] and CO/Pt(111)[80] in which the transient response of the internal C−O stretch vibration to picosecond laser heating of the substrate electrons was recorded. The measured transients are fitted by a model involving three coupled heat baths (electrons, substrate lattice, and T-mode) with the corresponding coupling times. The lattice- T-mode coupling times τ are related to the lateral friction force F_f acting on the displacement normal coordinate Q of a molecule with mass m by $F_f = -m\dot{Q}/\tau$.[31] For a dense c(2×2) layer of CO/Cu(001) at T_S = 100 K the overall characteristic coupling times of the T-mode to both

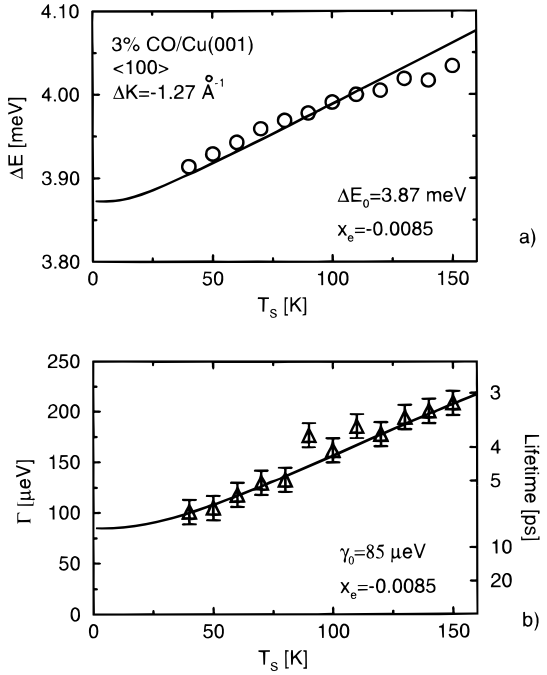

Figure 11. Temperature dependence (a) of the measured energy of the fundamental frustrated translational mode and (b) of the deconvoluted peak width (FWHM) for 3% CO/Cu(001).[56] The parallel momentum transfer is $\Delta K = -1.27$ Å^{-1}. The solid line shows the results of a calculation based on a simple anharmonic model, which has been adjusted to fit both sets of data.

the hot electrons and to the heated phonons is reported to be $\tau = 2$ ps. The individual contributions from electrons and phonons were estimated to be $\tau_e = 5.1$ ps and $\tau_{latt} = 4.2$ ps,[78] respectively.

For vibrational lifetimes in the low picosecond range, the natural line width γ of the vibrational mode should exhibit a significant broadening $\gamma (= \hbar/\tau)$ of about 0.3 meV.[31] High-resolution helium scattering from physisorbed rare gases on silver[150] or platinum[81,82] demonstrated that lifetime broadening effects can be measured directly by a careful peak-shape analysis. More recently this method has been applied to the T-mode for CO/Cu(001)[56] and Na/Cu(001).[2,71,83]

Figure 11 shows some recent results for the T-mode peak energy $\hbar\omega$ and the peak width γ as a function of the surface temperature T_S obtained for a small concentration of 3% CO on Cu(001).[56] The peak position shows a slight 2.5% shift to higher energy transfers with an increase of surface temperature from 40 to 150 K instead of the expected small decrease which is found for the Rayleigh phonons on the clean surface.[84] The observed energy shift can be fit by a linear dependence $\hbar\omega = a + bT$ with $a = 3.88 \pm 0.005$ meV and $b = (1.04 \pm 0.05)\ \mu$eV/K. The width γ also shows a distinct increase with temperature, which can be fitted again by a linear dependence $\gamma = \alpha + \beta T$ with $\alpha = 55 \pm 5\ \mu$eV and $\beta = (1.04 \pm 0.08)\ \mu$eV/K. The observed temperature-dependent vibrational energy shift is attributed to the anharmonicity of the lateral CO−copper potential. Assuming a positive anharmonic contribution $V_{anh}(x) \propto x^4$ instead of the usual negative term found for the vibrations of free molecules the observed temperature dependencies of both the peak energy and the peak

width can be well described by a simple model calculation which is shown as the solid curve in Figure 11.[56] It should be noted that the anharmonic model used allows the determination of an overall coupling time only at $T = 0$ K. The extrapolated values for the energy transfer and for the peak width to 0 K are $\hbar\omega_0 = 3.87 \pm 0.01$ meV and $\gamma_0 = 85 \pm 10$ μeV, respectively. The 0 K extrapolated T-mode peak width γ_0 corresponds to a vibrational lifetime $\tau = \hbar/\gamma_0 = 8$ ps, which is in reasonable agreement with the theoretical predictions for the T-mode substrate phonon bath coupling of 14 ps made by Persson and Ryberg.[31] The much smaller value of $\tau = 2$ ps obtained by Germer et al.[78] for the dense c(2×2) layer may be due to a significant contribution of adsorbate−adsorbate interactions to the T-mode vibrational lifetime and differences in the surface temperatures. As will be shown in the following section, these interactions can significantly change the adsorbate dynamics.

B. Adsorbate−Adsorbate Interactions

The presence of interactions between atoms and molecules adsorbed on surfaces is of major relevance for understanding adsorbate structures, their thermodynamic properties, and their mobility and reaction kinetics. As in the gas phase, molecules on surfaces interact at large distances via both van der Waals-type interactions and Coulombic forces and, at short range, via exchange forces. These are referred to as *direct* interactions. In addition, two different types of *indirect* interactions mediated through the substrate have been predicted theoretically. For one the surface affects the interactions between chemisorbed molecules via modifications of the electrons within the molecules and in the nearby surface area. On metals, any charge redistributions are screened very efficiently, and a rather rapid fall-off of charge-mediated interactions is expected. In particular, Lau and Kohn showed that within the jellium model the electronic interaction between two adsorbate atoms must decay asymptotically as $\cos(2k_F R)R^{-5}$.[9] As has been pointed out first by Feibelman and Hamann, this interaction is too localized to explain the surprising efficiency of catalyst poisons or promotors.[10] As an alternative mechanism they proposed that the long-range electronic interactions are affected by the Fermi-level density of states, which is not as rapidly screened out and can be modified over large distances.[10]

Moreover the adsorbed molecules can cause local elastic distortions in the substrate lattice, which due to their slow R^{-3} decay can also contribute significantly to the adsorbate−adsorbate interactions.[18−21] The indirect interactions are inherently complex and difficult to treat from first principles. There is, for example, no reason to expect pairwise additivity of these interactions when more than two adsorbed particles are involved.[85,86]

On the experimental side, at present, probably the most direct information on adsorbate interactions comes from spectroscopically determined vibrational dispersion curves of the frustrated translational and rotational modes of ordered adsorbates. The measured dispersion curves can be analyzed with lattice dynamical calculations, which are usually based on a simple Born−von Karman type of force constant model. As a typical example for such dynamical adsorbate−adsorbate interactions we describe in the following section a recent investigation of the adsorbate dynamics of a dense c(2×2) layer of CO on Cu(001).

There is now some experimental evidence that the substrate-mediated adsorbate interactions may be more subtle and do not always lead to a "dynamically" correlated adsorbate motion as indicated by dispersive vibrational modes. As a nice example for such "static" substrate-mediated adsorbate interactions, some very recent HAS results obtained for sodium on Cu(001) in the low-coverage regime are briefly described in section III.B.2.

1. Dynamical Interactions

As soon as the coupling between individual adsorbate molecules is introduced, the vibrational energies of the adsorbate layer will aquire a dependence on the parallel wavevector ΔK.[87] One of the first experiments to reveal the dispersion of an external adsorbate mode out to the Brillouin zone boundary was obtained 11 years ago by EELS for a c(2×2) layers of atomic oxygen adsorbed on Ni(001).[88] In this study, the mainly perpendicularly polarized adsorbate mode showed a strong dispersion between $\hbar\omega = 39$ meV at the zone center up to $\hbar\omega = 50$ meV at the zone boundary. These data in combination with detailed HAS data obtained later in the acoustic region of the dispersion curve supplied evidence for strongly repulsive O−O interactions within the oxygen layer.[89]

Surprisingly most of the HAS studies of the dispersion curves of the external modes for molecular adsorbates on both metal and insulator substrates show very little dispersion. One of the few systems showing dispersion is the T-mode of the c(2×2) structure of CO/Cu(001) which is shown in Figure 12. In both the ⟨100⟩ and ⟨110⟩ azimuths two modes with nearly the same frequencies are observed which are associated with the 4 meV frustrated translational mode of the isolated CO (see section III.A). The dispersionless branch located at $\hbar\omega = 4$ meV is assigned to the inelastic scattering from CO molecules near vacancies in the c(2×2) layer, which due to their large cross section contribute significantly to the HAS signal.[8] The other branch shows dispersion from the same value of $\hbar\omega = 4$ meV at the zone center up to 5.6 meV at the zone boundary in the ⟨110⟩ azimuth ($\Delta K = 1.23$ Å^{-1}) and also at the new adsorbate related zone boundary at $\Delta K = 0.87$ Å^{-1} in the ⟨100⟩ azimuth.

Since the dispersion curves of the frustrated translational mode in the c(2×2) CO overlayer overlap only in a small part of the Brillouin zone with the substrate bulk dispersion, the vibrational amplitude is mainly localized in the CO layer, and in a first approximation the motion of the underlying lattice can be neglected. Then the CO molecules can be represented by a two-dimensional square grid of identical particles of mass M connected by springs with each other and with the rigid substrate (see Figure 13).[8] These springs provide for radial (β) and

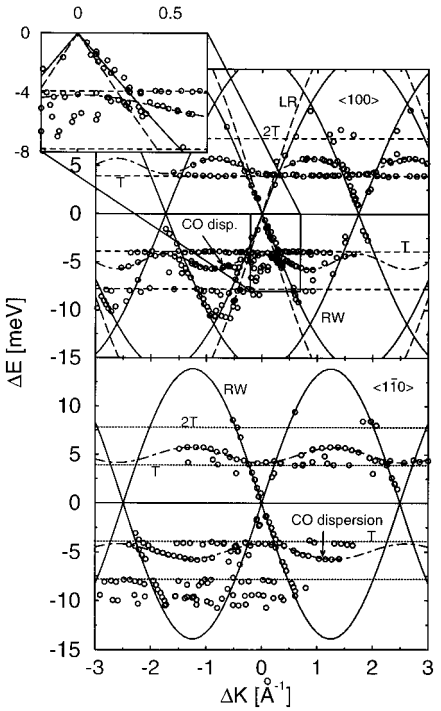

Figure 12. The dispersion curves of inelastic features as seen with HAS on a c(2×2) layer of CO ($\theta = 0.5$) on Cu(001) (a) along the ⟨100⟩ direction and (b) along the ⟨110⟩ azimuth. The data have been taken with incident energies of $E_i = 11.5$ and 17 meV, respectively, and a surface temperature $T_S = 50$ *K*.[48] The dash-dotted lines are the result of the simple lattice dynamical model calculation described in the text. The inset in part a shows an enlargement of the region in which the T- and RW-modes cross revealing a hybridization induced splitting.

tangential (α) force constants. They are related to the intermolecular potential $V(R)$ by the simple relationships

$$\beta = V''(R) \tag{8}$$

$$\alpha = \frac{V'(R)}{R} \tag{9}$$

where $V'(R)$ and $V''(R)$ denote first and second derivatives with respect to the intermolecular distance R. The dynamical matrix for this model can be easily solved, yielding the dispersion curves for the longitudinal modes for the two symmetry directions:

$$\langle 100\rangle: M\omega_L^2 = \alpha_1 + 4\beta_0 \sin^2\frac{aQ}{2} \tag{10}$$

$$\langle 110\rangle: M\omega_D^2 = \alpha_1 + 4(\beta_0 + \alpha_0) \sin^2\left(\frac{a'Q}{2}\right) \tag{11}$$

where a and a' are the corresponding lattice spacings. The force constants α_0, β_0, and α_1 are determined by fitting eqs 10 and 11 to the measured dispersion curves. As shown in Figure 12, the calculated dispersion curves fit the experiments over a large part of the Brillouin zone. Interestingly, the maximum frequency of the dispersive mode at the zone boundary is nearly identical in both the ⟨100⟩ and ⟨110⟩ directions, which by comparison of eqs 10 and 11 implies that $\alpha_0 \approx 0$. For the remaining parameters α_1 and β_0 we find $\alpha_1 = 1.7$ N/m and $\beta_0 = 0.2$ N/m. The vanishingly small tangential CO−CO force constant $\alpha_0 \equiv V'_{CO-CO}(R)$ implies that the c(2×2) CO−

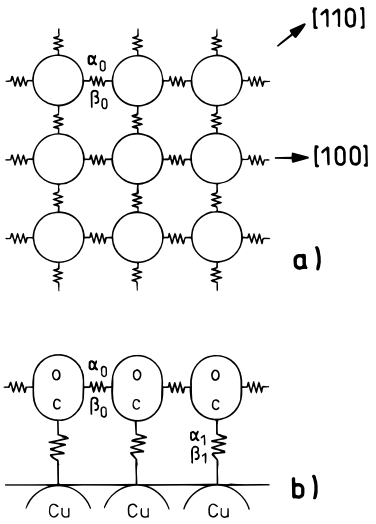

Figure 13. Schematic diagram of the simple model used to simulate the dispersion of the frustrated translation mode of a c(2×2) overlayer of CO on Cu(001):[8] (a) top view and (b) side view. The CO molecules and the copper substrate are assumed to be rigid. The coupling of the CO molecules to the substrate is modeled by the radial force constant β_1 (acting perpendicular to the surface) and the tangential force constant α_1 (acting parallel to the surface). The intermolecular coupling is represented by a radial force constant β_0 and a tangential force constant α_0 between nearest neighbors.

CO nearest neighbor distance of 3.61 Å corresponds practically to the minimum of the intermolecular potential. This interpretation has been recently supported by a transfer matrix analysis of desorption isotherm data for CO adsorbed onto different low-index copper surfaces.[90] Interestingly, the latter analysis exhibited strong evidence for a dominating contribution of indirect phonon-mediated lateral interactions, whereas direct dipole−dipole interactions and dispersion interactions are estimated to be relatively small.

More details on the coupling of the adsorbate molecules to the substrate are available from the splitting in the energies of the T-mode and RW mode at the point in Δ*K*-space where these two modes intersect each other (see inset in Figure 12). The lattice dynamical description of this hybridization induced splitting yields direct information on the damping of the adsorbate T-mode by the substrate Rayleigh mode, which is analyzed in ref 48.

Further information about possible adsorbate−substrate interaction mechanisms can be derived from a comparison of the tangential CO−Cu force constants α_1 for the dense c(2×2) layer with the corresponding value for isolated adsorbates (see section III.A. The fact that α_1 is identical in both cases within the experimental accuracy implies that the adsorbate−substrate potential is not affected by the adsorbate interactions. As will be shown in the following section, this behavior is not always observed, and in some cases significant coverage-dependent changes in the adsorbate−substrate potential are found.

2. Chemical Shifts of Adsorbate T-Mode Frequencies

The rather weak lateral interactions observed for adsorbed CO molecules are consistent with the

relatively weak binding energy and the comparatively small net charge transfer between the CO molecules and the surface as suggested by the small work function changes of typically $|\Delta\Phi| \lesssim 0.5$ eV upon adsorption.[6] Such arguments would suggest that much stronger interactions are expected for the chemisorption of alkali atoms on metal surfaces, for which very strong coverage-dependent changes in the work function[96] and the binding energy[91] are known. In the following we will present some recent HAS results obtained for sodium adsorbed on Cu(001). For this system a work function decrease by as much as $\Delta\Phi = 1.9$ eV is observed,[92] which is attributed to a strong polarization of the adsorbed sodium atoms.[93] The significant charge accumulation between the sodium atoms and the metal surface leads to the formation of strong dipole moments, which even at large adsorbate separations have been invoked to explain lateral interactions.[94]

These considerations are compatible with the existence of ordered structures often observed for very low coverages of alkali atoms on metal surfaces.[95,96] As an example, Figure 14a shows an angular distribution taken at a low 12.5% ML coverage of Na/Cu(001) along the ⟨100⟩ azimuth[48] at a surface temperature of $T_S = 50$ K. The sharp diffraction peaks observed in this angular distribution and further diffraction scans along other azimuths indicate the formation of an ordered c(2√2×4√2)R45° layer as predicted for a repulsive dipole−dipole interaction between the adsorbed alkali atoms.[95] The presence of the well-ordered c(2√2×4√2)R45° commensurate structure at these low coverages is very useful for characterizing the overlayer dynamics since the Brillouin zone is well defined, and measured phonon dispersion curves can be unambigously interpreted. Figure 14b shows the dispersion curve of the T-mode measured for the c(2√2×4√2)R45° Na overlayer. Assuming a direct repulsive dipole−dipole interaction energy $2\mu^2/R^3$ the experimental uncertainity on the extent of dispersion places an upper limit on the strength of the atomic dipole moment of $\mu < 3$ Debye.[48] This is consistent with the dipole moment $\mu_0 = 2.8$ Debye determined from the change in work function measurements with coverage.[97]

In Figure 14 it is also seen that the average energy of the T-mode depends strongly on the coverage. For example compared to a 0.8% coverage where the distance between atoms is 32 Å the energy is shifted upward by about 0.8 meV for the 12.5 Å coverage. An extensive analysis of the coverage dependence of the energetic shift reveals that it depends approximately linearly on the coverage between 0.8 and 12.5%.[48] Since this shift is much greater than the expected dispersion it cannot be explained by the direct dipole−dipole interaction. Interestingly the upward energy shift with coverage is also observed at the zone center. Since at the zone center the vibrations correspond to a rigid lateral translation of the entire overlayer, this observation also rules out that this shift is due to a dynamical coupling via direct adsorbate−adsorbate interactions. The vibrational energy shift with coverage must therefore be attributed to an indirect interaction mediated by the substrate. Consequently, even at the rather large

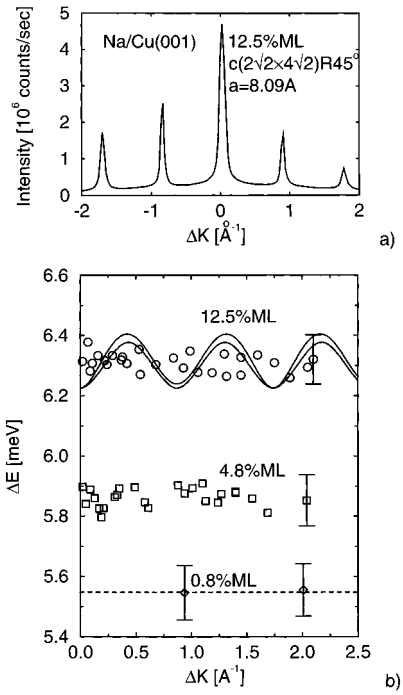

Figure 14. HAS measurements of the structure and dynamics of submonolayer films of Na/Cu(001) in the submonolayer coverage regime.[48] The angular distribution (a), taken along the ⟨100⟩ direction at a coverage of 12.5% ML, shows the formation of a well-ordered c(2√2×4√2)-R45° layer at a surface temperature of $T_S = 50$ *K*. The incident beam energy was $E_i = 20$ meV. (b) The measured vibrational T-mode frequencies for the same c(2√2×4√2)-R45° structure are plotted as a function of ΔK. All data points have been derived by extrapolating the phonon energies to $T_S = 0$ *K*. The solid line curves are from a lattice dynamical calculation for two domains of the ordered layer assuming a direct repulsive dipole−dipole interaction (dipole moment $\mu_0 = 2.8$ Debye). Within the experimental accuracy of 0.2 meV, as indicated by the error bar at $\Delta K = 1$ Å^{-1}, the data cannot rule out the presence of a small dispersion. For comparison, also the average T-mode energies obtained at lower coverages of 0.8% and 4.8% of a monolayer are shown by horizontal lines. The large downward shift with decreasing coverage is attributed to a strong substrate mediated interaction.

adsorbate nearest-neighbor distance of $d_{Na-Na} = 8.09$ Å for the c(2√2×4√2)R45° structure this substrate-mediated interaction dominates over the direct Coulombic dipole−dipole interaction. It should be noted, however, that the observed vibrational shifts correspond to only a rather small fraction of the total vibrational energy, indicating that the coupling through the substrate is small compared to the lateral holding potential.

The microscopic mechanism of this indirect interaction is currently not understood. It may originate from coverage-dependent modifications of the Fermi surface of the copper substrate as predicted by Einstein and Schrieffer.[15]

C. Complex Systems

The experimental techniques described above for rather simple adsorbate systems have recently been applied to larger, more complex molecules and to substrates with larger unit cells. Well-known examples of the latter are the physisorption of simple molecules on ionic crystals, which has recently at-

tracted considerable experimental and theoretical interest.[98] As a typical and relatively well understood example we will describe in the following some recent results for the adsorption of CO_2 on NaCl(001). Recently also some very promising HAS experiments have been performed on alkane molecules adsorbed on Cu(001[100] and this work is briefly described in section III.C.2.

1. CO_2/NaCl

Whereas the lateral interactions of adsorbates on metal surfaces turned out to be rather subtle due to the metal electrons, one may anticipate a much simpler behavior for the adsorption on insulating substrates. The interactions between adsorbate and substrate are of electrostatic and van der Waals nature, involving essentially additive two-body interactions.[102] In this sense, the physisorption of simple molecules on ionic substrates is more amenable to a fundamental interpretation with present day theoretical modeling.[103] For CO_2/NaCl(001), for example, both the structure and several characteristic vibrational frequencies have been described quite accurately by potential energy calculations of Heidberg et al.[104] These results are in good agreement with structural studies based on LEED,[105] IRS[106] and helium diffraction.[107,108] A (2×1) superstructure with two CO_2 molecules per unit cell with a tilt angle $\theta = 26°$ relative to the surface normal and an intermolecular azimuthal angle $\phi = 86°$ is obtained.

The theoretical analysis of Heidberg et al. included also a prediction of the vibrational frequencies of the external modes at the zone center $\bar{\Gamma}$ corresponding to the in-phase vibration of all molecules.[104] For linear molecules there are five external modes since the rotation around the molecule axis cannot be excited. For two linearly adsorbed molecules per unit cell, altogether $5 \times 2 = 10$ librational modes are expected with vibrational energies in the range from 2.2 meV up to 8.9 meV. Over the large crystal area of >1 mm^2 probed by the incident helium atom beam two perpendicular domains of the c(2×1) superstructure are sampled and thus up to 20 low-energetic librational modes can be expected theoretically. Obviously the experimental investigation of such a large number of closely spaced, low-energetic vibrational modes represents a major challenge. However, in a recent HAS study most of the librational modes could be resolved over a large part of the Brillouin zone.[108,109] A representative series of TOF spectra converted to the energy transfer scale is shown in Figure 15 for an incident energy of $E_i = 14$ meV. The spectra show a large number of well-defined inelastic peaks due to the excitation of different librational modes of the CO_2 molecules. All peaks exhibit significant shifts and intensity variations with the incident angle, indicating the existence of strong vibrational dispersion. The modes are numbered in order of increasing energy at the zone boundary. The indices "a" and "b" added to the labels II and III have been chosen because the crossing of these modes suggest that the modes correspond to different domains or to different symmetries.[108]

The corresponding dispersion curves are displayed in Figure 16. The lines through the data points are

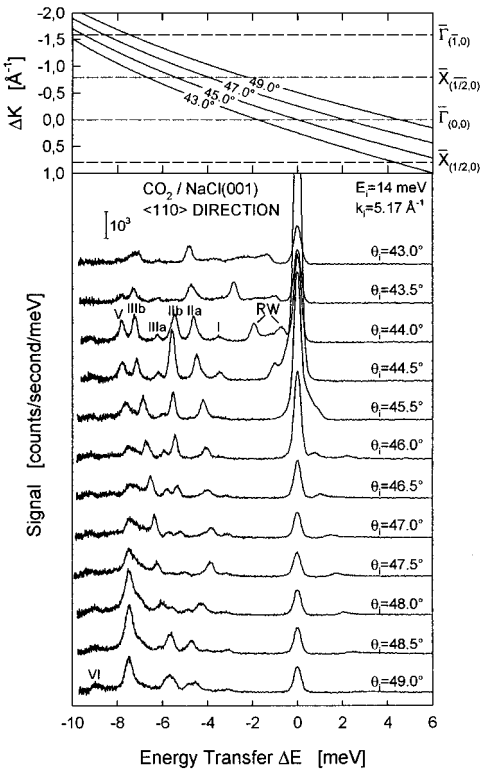

Figure 15. (b) A series of TOF spectra measured on a monolayer of CO_2 on NaCl(001) along the ⟨110⟩ direction for varying angles of incidence θ_i at $T_S = 30$ *K*. The incident beam energy is $E_i = 14$ meV. Scan curves for some of the incident angles θ_i are shown on the top in a. The substrate phonon excitation peaks are denoted by RW. The inelastic peaks due to the excitation of librational modes are labeled for the $\theta_i = 44°$ spectrum as described in the text.

intended as guides for the eye, in order to assist in classifying the different modes. The dispersion diagram shows eight branches with a significant dispersion. In the bulk band region (above the bulk band edge) the vibrational modes of the CO_2 layer can mix with the bulk bands and become resonances.[43] If the coupling is very strong their amplitude at the surface may be reduced to such an extent that they are no longer observed in the experiment as appears to be the case for the branches I, IIa, IIb, IIIb, and VI. In a very recent study Picaud, Hoang, and Girardet interpreted the measured dispersion curves for the CO_2 monolayer adsorbed on NaCl(001) on the basis of a semiempirical potential.[111] The various observed branches were identified in terms of coupled translational and rotational modes by solving the dynamical matrix of the adsorbate unit cell, for two perpendicularly oriented domains. In this study evidence for a large influence of the lateral adsorbate−adsobate interactions is found, leading to a strong hybridization of different motions. Altogether 20 distinct modes were predicted with energies at the Γ-point ranging from 1.5 to 13.3 meV. The fact that only eight branches are experimentally observed might be due to the difficulty to resolve some of the nearly degenerate modes. The coupling of the adsorbate vibrations with the substrate phonons, which was not included, is expected to have an important effect on the intensities and also on the frequencies of the adsorbate modes to the left of the Rayleigh mode in Figure 16.[108] The theory of Picaud et al.[111]

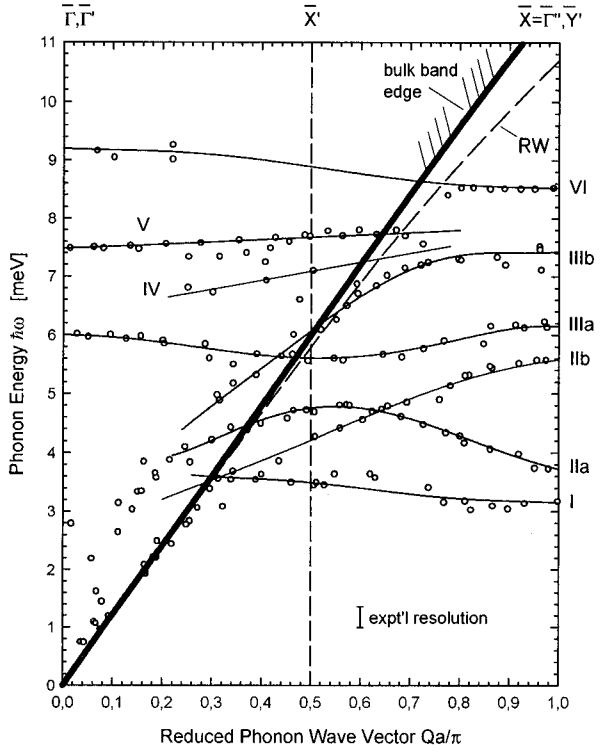

Figure 16. Measured phonon dispersion curves of one monolayer of CO_2/NaCl(001) along the ⟨110⟩ azimuth at T_S = 30 *K*, taken with E_i = 14 meV.[108] The Rayleigh mode RW and the bulk phonon edge are adapted from ref 110. The labeling of the dispersion branches corresponds to the labeling of the TOF features shown in Figure 15. The indices "a" and "b" of the labels II and III indicate branches of different domains or of different symmetry.

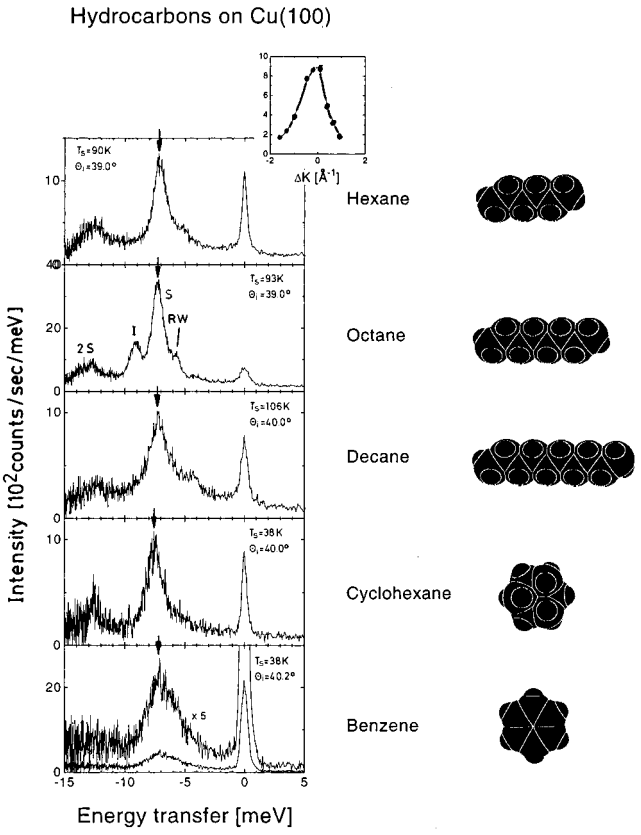

Figure 17. TOF spectra, converted into an energy-transfer scale, for monolayers of hexane, octane, decane, cyclohexane, and benzene on Cu(001).[100] The incident energy and angle were about 23 meV and 40° in all measurements. All spectra show in addition to a diffuse elastically scattered peak at $\Delta E = 0$ inelastic peaks due to the excitation of the perpendicularly polarized frustrated translation mode (S). In addition, for octane and decane an inelastic peak (I) due to the excitation of internal vibrations can be detected. The substrate Rayleigh phonon (RW) is seen in some of the spectra. The broad feature at ≈12.6 meV is assigned to an S-overtone excitation. The inset in the top right part shows the ΔK dependence of the excitation probability of the S_2 mode in the case of hexane. In the right column the structure of the molecules is shown.

is probably the most complete calculation of the dynamics of a complex adsorbate system performed so far. For a recent, similar experimental investigation of the dispersion curves for OCS on NaCl(001) the reader is refered to ref 99.

2. Alkanes on Cu(001)

At present, very little is known about the external vibrational modes of larger molecules. However, such information is of major relevance, e.g. for a microscopic understanding of the unique properties of hydrocarbons as boundary layer lubricants.[75] As a first step in this direction, recently the vibrations of the saturated hydrocarbons *n*-hexane, cyclohexane, *n*-octane, and *n*-decane adsorbed on a Cu(001) surface were investigated with HAS by Witte and Wöll.[100]

On the basis of the structural analysis of alkanes adsorbed on various low-index metal surfaces[101] it is expected that small hydrocarbon molecules on Cu(001) are adsorbed with their axis parallel to the surface (see Figure 17). A compilation of HAS energy loss spectra for monolayers of five different hydrocarbons [from top to bottom: *n*-hexane (C_6H_{14}), *n*-octane (C_8H_{18}), *n*-decane ($C_{10}H_{22}$), cyclohexane (C_6H_{12}), and benzene (C_6H_6)] is shown in Figure 17. Very recent measurements taken on the smaller hydrocarbons methane, ethane, and ethene exhibited almost identical spectra (ref 112; see also Table 5). Interestingly, the spectra are much simpler when compared to the case of CO_2 described in the preceding section: In all cases one dominant inelastic peak is observed within a narrow energy range between 6.8 meV and 7.3 meV. In addition, for octane a second adsorbate mode at an energy transfer of ΔE = 9.2 meV (*I*) is detected. The adsorbate modes are well separated from the substrate Rayleigh mode (RW).

In order to assign the modes, a careful analysis of the vibrational intensities as a function of the parallel wavevector transfer was performed.[100] As shown in the inset in Figure 17 for the example of hexane, the inelastic intensity decreases rapidly with increasing parallel wavevector transfer. The observed sharp peaking of the intensity at $\Delta K = 0$ is only compatible with a perpendicular polarization of the *S* peak centered at about 7 meV. Since the internal mode is seen in some of the systems at the expected energy of 9.2 meV, the peak at 7 meV is attributed to an external mode. Furthermore Witte and Wöll argue that the nearly identical S mode frequencies for all the alkanes[100] is due to a compensation of the effect of the length of the hydrocarbon molecule by the

Table 3. T-mode Frequencies of CO Molecules Adsorbed on Metal Surfaces[a]

system	structure	site	E_{Ad}/(kJ/mol)	$\hbar\omega$ (meV)	ref(s)	comments
CO/Cu(111)	isolated	t	−	4.15	122	
CO/Cu(001)	isolated	t	69 (ref 123)	3.94	8, 56	
				42.8 (ν_2)	6	C−Cu stretch
				35.3 (ν_3)	7	frust. Rot.
				257.8 (ν_1)	6	C−O stretch
		b?		5.3 weak	125	
	c(2×2)	t	−	$\overline{\Gamma M}$: 3.94 → 5.6	8	
CO/Cu(112)	isolated	t	−	3.0	118	step-edge ads.
	c(4×1)	t+b	−	4.1	118	step-edge ads.
CO/Ni(001)	isolated	t+b	125 (ref 123)	4	128, 5	broad peak
	c(2×2)	t	−	4	128, 5	
				59.5 (ν_2)	129	C−Ni stretch
				256.5 (ν_1)	129	C−O stretch
CO/Ni(111)	*c*(4×2)	b	−	11.8	120	
CO/Ni(110)	isolated	t?	−	∼3.9	130	
	c(2×1)	b; tilted	−	$\overline{\Gamma X}$: 14 → 7	119, 130	downward disp.
				$\overline{\Gamma Y}$: 14 → 7		14 meV = 2 × 7 meV?
CO/Pt(111)	isolated	t	−	6	32	
		t	−	59.5 (ν_2)	131	
		t	−	51.0 (ν_3)	5	
	($\sqrt{3}\times\sqrt{3}$) R30°	t	−	6.0	32	
	c(4×2)	b	133 (ref 124)	7.4	32	
CO/Rh(111)	isolated	t	−	5.75	126	
	($\sqrt{3}\times\sqrt{3}$) R30°	t	134 (ref 6)	5.45	126	8 overtones
	(2×2)3CO	t+b	−	$\overline{\Gamma K}$: 5.75 → 5.95		1. overtone dominant
CO/Ru(0001)	isolated	t	160 (ref 127)	6.1	122	
	($\sqrt{3}\times\sqrt{3}$) R30°	t	175 (ref 127)	5.7	122	6 overtones
CO/H/Ru(0001)	−	−	−	6.7	122	
CO/O_2/Rh(111)	saturation	−	−	8.4	132	
	isolated	−	−	7.7		
CO/Ir(001)	(1×1)	t	−	6.6	133	
	(5×1)	t	−	6.6		
CO/Al(111)	isolated	−	−	4.3	134	CO flat?
CO/Fe(110)	c(4×2)	t	155 (ref 6)	4.8	135	
CO/W(110)	p(5×1)	t	86 (ref 6)	8, 13, 16	136	

[a] For Cu(001), Ni(001), Rh(111), and Ru(0001) the frequencies of some of the other modes are listed. On the (001) and (111) surfaces of fcc metals ν_1 indicates the internal C−O stretch mode, ν_2 is the carbon−metal stretch mode and ν_3 is the frustrated rotation. The sites are abbreviated by "t" (on-top), "b" (bridge), and "h" (hollow) (see Figure 1). For the dispersive modes the frequencies are listed first at the zone center and at the zone with an arrow (→) between.

corresponding increase in effective mass. Also the fact that virtually identical S-mode energies are observed for cyclohexane and benzene can be rationalized by considering the similarity in the molecular polarizabilities which is responsible for the van der Waals physisorption forces of these molecules.[100]

A similar analysis performed for the weaker inelastic peak designated by I in Figure 17 seen for octane at an energy transfer of $\Delta E = -9.2$ meV, indicates that this feature cannot be related to an external molecular vibration.[100,114] Therefore these peaks are assigned to the excitation of internal molecular vibrations, as predicted at these low energies by previous force-field calculations.[113]

Surprisingly, energy losses which can be related to a hydrocarbon frustrated translation parallel to the surface have only been observed for ethene,[112] but for none of the other hydrocarbons. Generally one may expect a rather low vibrational frequency for the T-modes because of the misfit between the alkane corrugation and the substrate corrugation. In this case, the experimental resolution places an upper limit of ≈0.3 meV on the energy of the T-mode parallel to the surface.[100] The exceptional behavior of ethene may have to do with the strong dipole moment acquired by the molecule upon adsorption on metal surfaces.[115]

IV. Survey of Available Data

At the present time the amount of data concerning the low-energy external modes of molecules adsorbed on single crystal surfaces is still small enough to allow a rather comprehensive compilation. In order to compare equivalent adsorption systems, the data are coarsely divided into five groups: CO molecules adsorbed on metal substrates (Table 3), other small molecules adsorbed on metals (Table 4), hydrocarbons adsorbed on Cu(001) (Table 5), molecules adsorbed on insulating substrates (Table 6), and finally a small selection of atomic adsorbate systems (Table 7).

For CO on metal surfaces, the available data base is large enough to extract the following trends. As can be seen in Table 3 for the cases of CO on Cu(001), Ni(001), and Pt(111), the T-mode energies ($\hbar\omega \approx 4-6$ meV) are by 1 order of magnitude smaller than the vibrational energies of the carbon−metal stretch mode ($\hbar\omega(\nu_2) \approx 40-60$ meV). As mentioned already in the Introduction, this fact simply reflects the rather weak lateral corrugation of the potential energy surface which typically amounts to only about 3−10% of the binding energy (see section III.A).

Generally the vibrational energies of all librational modes, ν_2, ν_3, and ν_4 increase with the binding energy E_{Ad}. Significant deviations from this rule are ob-

Table 4. T-mode Frequencies of Molecular Adsorbates Other than CO on Metal Substrates

adsorbate system	structure	site	$\hbar\omega$ (meV)	ref	comments
NO/Rh(111)	isolated	(b)	11.5 (broad)	137	
	isolated	(b)	7.5 (weak)	137	
	$c(4\times2)$	b	7.45	137	
	(2×2) 3NO	b+t	7.45	137	
	(2×2) 3NO	b+t	$\overline{\Gamma K'}$: 13.5 → 11	137	Downward disp.
	(2×2) 3NO	b+t	50.2, 60.1(⊥)	138	
NO/Pd(110)	−	b	8.43	139	
NO/Cu(001)	isolated	−	6.3 (broad)	126	
	$p(2\times2)$	−	6.4 (broad)	126	
CO_2/Rh(111)	$(\sqrt{3}\times\sqrt{3})$?	−	ca. 7	132	$T_S = 110$ K
		−	5.8		$T_S = 50$ K
CO_2/Ni(110)	(2×2)	b	$\overline{\Gamma X}$: 5−14 (3 modes)	132	Dispersion
			$\overline{\Gamma X}$: 4.5, 6.1	132	
NH_3/Rh(111)	(2×2)	−	12.7, 14.5	137	
NH_3/Fe(110)	−	t	10	135	
N_2/Ni(110)	isolated	b	4.9	140	
		t	5.9		
N_2/Ni(001)	isolated	t	6.8	140	
O_2/Rh(111)	$p(2\times2)$	h	7.7	132	$T_S = 250$ K
	+ facets		6.9		$T_S = 100$ K
C_6H_6/Rh(111)	$(2\sqrt{3}\times3)$	t	13.2	141	
	$(2\sqrt{3}\times3)$	t	42.8, 68.2 (⊥)	142	
C_6H_6/CO/Rh(111)	$(2\sqrt{3}\times4)$	t	12.9 (∥)	141	

Table 5. Low-Energy Librational Modes of Hydrocarbons Adsorbed on Cu(001)[a]

adsorbate system	$T_{des}(K)$	$\hbar\omega$ (meV)	ref	comments
CH_4/Cu(001)	55	6.5 (⊥)	112	
C_2H_4/Cu(001)	80−140	6.8 (⊥)	112	extended desorption
		4.9 (∥)	112	
C_2H_6/Cu(001)	92	7.0 (⊥)	112	
C_6H_{14}/Cu(001)	175	6.8 (⊥)	100	
C_8H_{18}/Cu(001)	220	7.0 (⊥)	100	
		9.2 (I)	100	
$C_{10}H_{22}$/Cu(001)	250	7.0 (⊥)	100	
C_6H_{12}/Cu(001)	160	7.3 (⊥)	100	
C_6H_6/Cu(001)	170	7.3 (⊥)	100	

[a] For the alkanes (C_n H_{2n+2}) the T-modes with parallel polarization have not been observed. Their energies are estimated to be lower than 0.3 meV.[100] The internal bend mode of octane is denoted by "I".

served, however, for the T-modes of CO/Ni(001) and CO/Ni(110), where despite the rather large binding energy of 125 kJ/mol rather low T-mode vibrational energies ($\hbar\omega \approx 3.9-4$ meV) are found.

Considering the T-modes on the different copper surfaces, a clear influence of the coordination of the adsorption site on the vibrational energy is found: The highest energy $\hbar\omega = 4.15$ meV is measured for the (111) surface with its 6-fold coordinated on-top binding site. On the 4-fold coordinated on-top site of Cu(001) the T-mode energy is $\hbar\omega = 3.95$ meV, and on the very open Cu(211) surface an energy of $\hbar\omega = 3.0$ meV is obtained. The latter value is compatible with the expectation of a predominant adsorption on low-coordinated step edge sites.[54,116,117] Further evidence for this trend has been found by recent measurements of the T-modes of CO molecules adsorbed on single Cu adatoms ($\hbar\omega = 2.5$ meV) and step edges ($\hbar\omega = 3.2$ meV) created on a Cu(001) surface by modest sputtering.[118]

The very consistent coordination dependence obtained on copper surfaces described above raises some questions about some recent EELS experiments. For example, the practically perfect azimuthal isotropy observed by EELS for the dispersion curves of the dense (2×1) layer of CO on the rather anisotropic Ni(110) surface[119] is not consistent with the trends discussed. This inconsistency and also the unusual softening of the adsorbate dispersion ($\hbar\omega_{\bar{\Gamma}} > \hbar\omega_{\bar{Y}}$) suggests the possible existence of additional branches of the T-mode dispersion curves at lower energies which were not resolved in the EELS spectra. Similar problems may exist concerning the interpretation of EELS measurements performed on CO/Ni(111),[120] where a dispersionless feature in the measured dispersion curve at $\hbar\omega = 11.8$ meV was assigned to the low-energetic ν_6 mode of bridge-bonded CO molecules with neglible lateral interactions. Considering the much lower vibrational energies of $\hbar\omega \approx 4$ meV observed for CO/Ni(001) and for low coverages of CO/Ni(110) there is no reason to expect much higher T-mode energies for CO on Ni(111) surfaces. Thus in this case it also appears that only an overtone was detected by EELS.

V. Summary and Outlook

In recent years the relatively new experimental technique of inelastic He atom time-of-flight spectroscopy has been applied to the investigation of the lowest energy thermally excited vibrations of atoms and molecules adsorbed on single-crystal surfaces. Although at present only a relatively small number

Table 6. T-Modes of Molecular Adsorbates on Ionic Insulator Substrate[a]

adsorbate system	structure	site	$T_{des}(K)$	$\hbar\omega$ (meV)	ref(s)	comments
H_2O/NaCl(001)	p(1×1)	−	154	5.5(∥)	143	
H_2O/MgO(001)	c(4×2)	−	215	23	144	
OCS/LiF(001)	−	−	−	6, 8	145	
OCS/NaCl(001)	p(2×1)	−	80	3−10 (8 modes)	99	dispersion
CO/NaCl(001)	p(2×1)	t_{Na}	50−60	7.5	146	tilted
				2.5−4, 4.5	146	weak
CO/MgO(001)	$c(4\times2)$	t	59	9, 10.3	147	
	isolated	t	−	9	147	
CO_2/MgO(001)	$2\sqrt{2}\times\sqrt{2}$R45°		≳80	9, 12	148	
CO_2/NaCl(001)	p(2×1)	−	≈80	2−9 (8 modes)	109, 108	dispersion
CH_4/NaCl(001)	p(2×2)	−	≈50	4−16 (7 modes)	146	
C_2 H_2/NaCl(001)	$p(\sqrt{2}\times3\sqrt{2})$R45°	−	85	8	149	
	$p(\sqrt{2}\times7\sqrt{2})$R45°	−	−	14.5	149	

[a] The desorption temperatures T_{des} have been determined with HAS by measuring the strongly coverage dependent specular intensity while ramping the surface temperature with a rate of $\beta \approx 0.1$ K/s.

Table 7. Vibrational Mode Frequencies of Selected Atomic Adsorbates

adsorbate system	structure	site	$\hbar\omega$ (meV)	ref(s)	comment
Ar/Ag(111)	hex (IC)	−	3.8 (⊥)	150	
Kr/Ag(111)	hex (IC)	−	2.95 (⊥)	150	
Xe/Ag(111)	hex (IC)	−	2.8 (⊥)	150	
Ar/Pt(111)	−	−	4.85 (⊥)	81	
Kr/Pt(111)	−	−	3.9 (⊥)	81	
Xe/Pt(111)	$(\sqrt{3}\times\sqrt{3})$R30°	t	3.7 (⊥)	81	
Xe/Cu(001)	$(\sqrt{3}\times\sqrt{3})$R30°	−	2.7 (⊥)	151	
		−	0.2 → 2.3 (∥)	151	
Xe/C(0001)	$(\sqrt{3}\times\sqrt{3})$R30°	h	3.2 (⊥)	152	
Kr/C(0001)	$(\sqrt{3}\times\sqrt{3})$R30°	h	4.0 (⊥)	152	
Li/Cu(100)	isolated	h	35−37 (⊥)	153	
Na/Cu(100)	isolated	h	5.6 (∥)	2, 48	coverage dep.
			19 (⊥)	154	
K/Cu(100)	isolated	h	2.86 (∥)	114	
			12 (⊥)	154	
Cs/Cu(001)	isolated	−	0.65 (∥)	114	
	hex (IC)	−	0.65 → 5.6 (∥)	114	
	hex (IC)	−	6.8 (⊥)	114	
O/Ni(001)	c(2×2)	h	56 (∥)	155	
	c(2×2)	h	$\overline{\Gamma X}$: 39 → 51 (⊥)	155	
H/Ni(001)	p(2×2) H	h	74 (⊥)	156	

of adsorbate systems have been investigated the results of a number of recent exemplary studies demonstrate the great future promise of this technique. The measured energies of the frustrated translational modes make it possible to calculate the entropic contribution to the thermodynamics of adsorbates which in some cases may be important in determining adsorbate structures. These energies also provide unique insight into the curvature of the potential energy surface at the binding sites. In some dense film systems a dispersion or energetic shift with coverage is found which provides quantitative microscopic data on adsorbate−adsorbate interactions. The energetic widths of the inelastic peak also provide directly the coupling parameters describing the frictional coupling of the translational motion to the substrate heat bath. Related experimental measurements of the energetic width of the diffuse elastic peak provide detailed information on the microscopic mechansims of diffusion. The diffusion barriers complement the information on the potential surface in regions between binding sites. With this new information on potentials, frictional coupling parameters, and adsorbate−adsorbate interactions, detailed molecular dynamical studies of the motion of adsorbates on surfaces are now possible. Hopefully such simulations will ultimately advance our microscopic understanding of surface chemical reactions, adsorbate structures as well as more technically relevant issues such as friction and lubrication.

The techniques described here can also be applied to other fundamental problems. For example, phase transitions of adsorbates are expected to be driven by a softening of the longitudinal modes in the films. Such experiments have only been reported by neutron scattering for the 2D melting phase transition of monolayers of Ar adsorbed on graphite.[157] Such transitions are also accompanied by critical scattering which leads to a broadening in the elastic and inelastic peaks at temperatures very close to the critical temperatures. This has only been seen in a few instances with He atom scattering.[158,159] Another interesting area for future research is the study of mixed films with and without long-range order. For example coadsorbed Na and CO on Cu(001) reveals a highly ordered surface structure and a vibrational spectrum with new energy losses.[48]

Finally it should be mentioned that compared to other surface spectroscopic techniques helium atom scattering is still in its infancy. New sophisticated techniques such as the adaption of the neutron spin echo method for ^{3}He scattering open up the possibility of ultrahigh resolution experiments with $\Delta E \approx 10^{-8}$ eV.[160] Also recent improvements in using stepped surface echelette gratings as monochromators and energy analyzing devices now appear very promising.[161] In conclusion we hope we have convinced the reader that the field of surface molecular dynamics holds great promise for the future.

VI. Acknowledgments

We thank M. Bertino, J. Braun, A. Glebov, A. P. Graham, G. Lange, W. Silvestri, G. Witte, and Ch. Wöll for providing unpublished data and helpful discussions. We are very grateful to A. Graham, B. Gumhalter, and Ch. Wöll for a careful reading of the manuscript.

VII. References

(1) Gomer, R. *Rep. Prog. Phys* **1990**, *53*, 917.
(2) Ellis, J.; Toennies, J. P. *Phys. Rev. Lett.* **1993**, *70*, 2118. Ellis, J.; Toennies, J. P. *Surf. Sci.* **1994,** *317*, 99.
(3) Bertino, M.; Hofmann, F.; Steinhögl, W.; Toennies, J. P. *J. Chem. Phys.*, submitted for publication.
(4) Richardson, N. V.; Bradshaw, A. M. *Surf. Sci.* **1979**, *88*, 255.
(5) Hähner, G.; Toennies, J. P.; Wöll, Ch. *Appl. Phys.* **1990**, *A51*, 208.
(6) Campuzano, J. C. In *The Chemical Physics of Solid Surfaces and Heterogeneous Catalysis*, King, D. A., Woodruff, D. P., Eds.; Elsevier Science Publishers: Amsterdam 1990; Vol. 3A, pp 389 ff.
(7) Hirschmugl, C. J.; Williams, G. P.; Hoffmann, F. M.; Chabal, Y. J. *Phys. Rev. Lett.* **1990**, *65*, 480.
(8) Ellis, J.; Witte, G.; Toennies, J. P. *J. Chem. Phys.* **1995**, *102*, 5059.
(9) Lau, K. H.; Kohn, W. *Surf. Sci.* **1978**, *75*, 3629.
(10) Feibelman, P. J.; Haman, D. R. *Phys. Rev. Lett.* **1984**, *52*, 61.
(11) For a review see the article: March, N. H. *Interactions of Atoms and Molecules with Solid Surfaces*; Bortolani, V., March, N. H., Tosi, M. P., Eds.; Plenum: New York, 1990; p 1.
(12) Lang, N. D. *Phys. Rev. Lett.* **1981**, *46*, 842.
(13) Müller, J. E. *Phys. Rev. Lett.* **1990**, *65*, 3021.
(14) Zangwill, A. *Physics at Surfaces*; Cambridge University Press: Cambridge, 1988.
(15) Einstein, T. L.; Schrieffer, J. R. *Phys. Rev. B* **1973**, *7*, 3629.
(16) Kohn, W.; Lau, K. H. *Solid State Commun.* **1976**, *18*, 553.
(17) Crommie, M. F.; Lutz, C. P.; Eigler, D. M. *Nature* **1993**, *363*, 524.
(18) Lau, K. H. *Solid State Commun.* **1978**, *28*, 757.
(19) Prybyla, J. A.; Estrup, P. J.; Ying, S. C.; Chabal, Y. J.; Christman, S. B. *Phys. Rev. Lett.* **1987**, *58*, 1877.
(20) Tiersten, S. C.; Reinecke, T. L.; Ying, S. C. *Phys. Rev. B* **1989**, *39*, 12575.
(21) Tiersten, S. C.; Reinecke, T. L.; Ying, S. C. *Phys. Rev. B* **1991**, *43*, 12045.
(22) Nørskov, J. K.; In *The Chemical Physics of Solid Surfaces*; King, D. A., Woodruff, D. P., Eds.; Elsevier: New York, 1990; Vol. 6.
(23) Persson, B. N. J. *Surf. Sci. Rep.* **1992**, *15*, 1.
(24) Golze, M.; Grunze, M.; Unertl, W. *Prog. Surf. Sci.* **1986**, *22*, 101.
(25) Bandy, B. J.; Canning, N. D. S.; Hollins, P.; Pritchard, J. *J. Chem. Soc., Chem. Commun.* **1982**, 58.
(26) Yoshinobu, J.; Takagi, N.; Kawai, M. *Phys. Rev. B* **1994**, *49*, 16670.
(27) Grossmann, A.; Erley, W.; Ibach, H. *Phys. Rev. Lett.* **1993**, *71*, 2078.
(28) Schweizer, E.; Persson, B. N. J.; Tüshaus, M.; Hoge, D.; Bradshaw, A. M. *Surf. Sci.* **1989**, *213*, 49.
(29) Over, H.; Moritz, M.; Ertl, G. *Phys. Rev. Lett.* **1993**, *70*, 315.

(30) Gierer, M.; Bludau, H.; Over, H.; Ertl, G. *Surf. Sci.* **1996**, *346*, 64. Over, H.; Gierer, M.; Bludau, H.; Ertl, G. *Phys. Rev. B* **1995**, *52*, in press.
(31) Persson, B. N. J.; Ryberg, R. *Phys. Rev. B* **1985**, *32*, 3586.
(32) Lahee, A.; Toennies, J. P.; Wöll, Ch. *Surf. Sci.* **1986**, *177*, 371.
(33) Bée, M. *Quasileastic neutron scattering*; Adam Hilger: Bristol, 1988.
(34) Parker, S. F. *Spectros. Eur.* **1994**, *6/6*, 14.
(35) Stockmeyer, R.; Conrad, H. M.; Renouprez, A.; Fouilloux, P. *Surf. Sci.* **1975**, *49*, 45. Jobic, H.; Tomkinson, J.; Candy, J. P.; Foulilloux, P.; Renouprez, A. *Surf. Sci.* **1980**, *95*, 496.
(36) Chabal, Y. J. *Surf. Sci. Rep.* **1988**, *8*, 211.
(37) Chabal, Y. J. *Phys. Rev. Lett.* **1985**, *55*, 845.
(38) Hirschmugl, C. J.; Williams, G. P.; Persson, B. N. J.; Volokitin, A. I. *Surf. Sci.* **1994**, *317*, L1141.
(39) Ibach, H. *Electron Energy Loss Spectrometers*; Springer Series in Optical Sciences; Springer: Heidelberg, 1991. Kesmodel, L. L. In *Handbook of Surface Imaging and Visualization*; Hubbard, A. T., Ed., CRC Press: Boca Raton, FL, 1995 (in press). Erskine, J. L. *J. Vac. Sci. Technol.* **1986**, *A 4*, 1282.
(40) Heinz, K.; Müller, K.; In, *Structural Studies of Surfaces*; Springer Tracts in Modern Physics, Höhler, G., Ed.; Springer-Verlag: Berlin, 1982; Vol. 91.
(41) Frenken, J. W. M.; Toennies, J. P.; Wöll, Ch. *Phys. Rev. Lett.* **1988**, *60*, 1727. Frenken, J. W. M.; Hinch, B. J.; Toennies, J. P.; Wöll, Ch. *Phys. Rev. B* **1990-I**, *41*, 938.
(42) Frenken, J. W. M.; Hinch, B. J.; in *Helium Atom Scattering from Surfaces*; Hulpke, E., Ed.; Springer Series in Surface Science 27; Springer-Verlag: New York, 1992; p 287.
(43) Benedek, G.; Toennies, J. P. *Surf. Sci. Rep.*, in preparation.
(44) Toennies, J. P.; Winkelmann, K. J. *J. Chem. Phys.* **1977**, *66*, 3965.
(45) Brusdeylins, G.; Doak, R. B.; Toennies, J. P. *Phys. Rev. B* **1983**, *27*, 3662.
(46) Smilgies, D.-M.; Toennies, J. P. *Rev. Sci. Instrum.* **1988**, *59*, 2185.
(47) Skorupka, C. W.; Manson, J. R. *Phys. Rev. B* **1990**, *41*, 9783.
(48) Graham, A.; Hofmann, F.; Toennies, J. P. To be published.
(49) Engel, T.; Rieder, K. H. In *Structural Studies of Surfaces*; Springer Tracts in Modern Physics 91; Springer-Verlag: New York, 1982; p 55.
(50) Manson, J. R.; Celli, V. *Surf. Sci.* **1971**, *24*, 495. Celli, V.; Benedek, G.; Harten, U.; Toennies, J. P.; Doak, R. B.; Bortolani, V. *Surf. Sci.* **1984**, *143*, L376. Manson, J. R. *Phys. Rev. B* **1991**, ***43***, 6924.
(51) Bilic, A.; Gumhalter, B. *Phys. Rev. B* **1995**, *52*, 12307. Gumhalter, B. *Surf. Sci.*, **1995**, in press.
(52) Bertino, M.; Ellis, J.; Hofmann, F.; Toennies, J. P. *Phys. Rev. Lett.* **1994**, *73*, 605.
(53) Poelsma, B.; Verheij, L. K.; Comsa, G. *Phys. Rev. Lett.* **51**, 2410 (1983); *Surf. Sci.* **1985**, *152/153*, 851. Kern, K.; David, R.; Palmer, R. L.; Comsa, G. *Phys. Rev. Lett.* **1986**, *56*, 620. Kern, K.; Comsa, G. *Adv. Chem. Phys.* **1989**, *76*, 211.
(54) Borguet, E.; Dai, H.-L. *J. Chem. Phys.* **1994**, *101*, 9080.
(55) Haq, S.; Love, J. G.; King, D. A. *Surf. Sci.* **1992**, *275*, 170. Torbin, Yu. K. *Prog. Surf. Sci.* **1991**, *34*, 1. Tracy, J. C. *J. Chem. Phys.* **1972**, *56*, 2736.
(56) Graham, A.; Hofmann, F.; Toennies, J. P. *J. Chem. Phys.*, in press.
(57) Hu, P.; King, D. A.; Crampin, S.; Lee, M.-H.; Payne, M. C. *Chem. Phys. Lett.* **1994**, *230*, 501.
(58) Graham, A.; Hofmann, F.; Silvestri, W.; Toennies, J. P. To be published.
(59) Hofmann, F.; Schöllkopf, W.; Toennies, J. P. In *Chemical Dynamics of Transient Species*; Proceedings of the 38th Welch Foundation Symposium, 1994; p 197.
(60) Hinch, B. J.; Frenken, J. W. M.; Zhang, G.; Toennies, J. P. *Surf. Sci.* **1991**, *259*, 288. These measurements concentrated on the ΔK dependence of the quasielastic broadening. At $T_S = 820$ K a diffusion constant $D = 5 \times 10^{-6}$ cm^2/s has been found. Values for E_D and D_0 were not reported.
(61) van Hove, L., *Phys. Rev.* **1954**, *95*, 249.
(62) Levi, A. C.; Spadacini, R.; Tommei, G. E. *Surf. Sci.* **1982**, *121*, 504.
(63) Chudley, C. T.; Elliott, R. J. *Proc. Phys. Soc. London* **1961**, *77*, 353.
(64) Chen, L. Y.; Ying, S. C. *Phys. Rev. Lett.* **1993**, 71, 4361; *Phys. Rev. B* **1994**, *49*, 13838.
(65) Roop, B.; Costello, S. A.; Mullins, D. R.; White, J. M. *J. Chem. Phys.* **1987**, *86*, 3003.
(66) Lin, T. S.; Lu, H. J.; Gomer, R. *Surf. Sci.* **1990**, *234*, 251.
(67) Xiao, X.-D.; Xie, Y.; Shen, Y. R. *Phys. Rev. B* **1993-I**, *48*, 17452.
(68) Xiao, X.-D.; Xie, Y.; Jacobsen, C.; Galloway, H.; Salmeron, M.; Shen, Y. R. *Phys. Rev. Lett.* **1995**, *74*, 3860.
(69) Xiao, X.-D.; Xie, Y.; Shen, Y. R. *Surf. Sci.* **1992**, *271*, 295.
(70) Bertino, M.; Hofmann, F.; Steinhögl, W.; Toennies, J. P. To be published.
(71) Chen, L. Y.; Ying, S. C. *Phys. Rev. Lett.* **1993**, *71*, 4361.
(72) Ying, S. C. Private communication.
(73) Dobbs, K. D.; Doren, D. J. *J. Chem. Phys.* **1992**, *97*, 3722.
(74) Ala-Nissila, T.; Ying, S. C. *Prog. Surf. Sci.* **1992**, *39*, 227.
(75) Persson, B. N. J. *Phys. Rev. B* **1993**, *48*, 18140.
(76) Naumovets, A. G.; Vedula, Yu. S. *Surf. Sci. Rep.* **1985**, *4*, 365.
(77) Tully, J. C.; Gomez, M.; Head-Gordon, M. *J. Vac. Sci. Technol. A* **1993**, *11*, 1914.
(78) Germer, T. A.; Stephenson, J. C.; Heilweil, E. J.; Cavanagh, R. R. *J. Chem. Phys.* **1994**, *101*, 1704.
(79) Culver, J. P.; Li, M.; Jahn, L. G.; Hochstrasser, R. M.; Yodh, A. G. *Chem. Phys. Lett.* **1993**, *214*, 431.
(80) Germer, T. A.; Stephenson, J. C.; Heilweil, E. J.; Cavanagh, R. R. *Phys. Rev. Lett.* **1993**, *71*, 3327.
(81) Hall, B.; Mills, D. L.; Zeppenfeld, P.; Kern, K.; Becher, U.; Comsa, G. *Phys. Rev. B* **1989**, *40*, 6326.
(82) Zeppenfeld, P.; Becher, U.; Kern, K.; David, R.; Comsa, G. *Phys. Rev. B* **1990**, *41*, 8549.
(83) Graham, A.; Hofmann, F.; Cuccetti, A.; Toennies, J. P.; Ying, S. C. To be published.
(84) Benedek, G.; Toennies, J. P. *Phys. Rev. B* **1992**, *46*, 13643.
(85) Einstein, T. L. In *Chemistry and Physics of Solid Surfaces*; Vanselow, R., Ed.; CRC: Boca Raton, 1979.
(86) Einstein, T. L. *Langmuir* **1991**, *7*, 2520.
(87) Ibach, H.; Mills, D. L. In, *Electron Energy Loss Spectroscopy and Surface Vibrations*; Academic: New York, 1982.
(88) Szeftel, J. M.; Lehwald, S. *Surf. Sci.* **1984**, *143*, 11.
(89) Berndt, R.; Toennies, J. P.; Wöll, Ch. *Surf. Sci.* **1991**, *244*, 305.
(90) Wei, D. H.; Skelton, D. C.; Kevan, S. D. *Surf. Sci.* **1995**, *326*, 167.
(91) Rangelov, G.; Surnev, L. *Surf. Sci.* **1987**, *185*, 457.
(92) Lars Walldén, *Surf. Sci. Lett.* **1983**, *134*, L513.
(93) Bagus, P. S.; Pacchioni, G. *J. Chem. Phys.* **1995**, *102*, 879.
(94) Naumovets, A. G. *Sov. Sci. Rev. A Phys.* **1984**, *5*,443.
(95) Diehl, R. D.; McGrath, R. *Surf. Rev. Lett.* **1995**, *V2*, 387.
(96) *Physics and Chemistry of Alkali Metal Adsorption*; Bonzel, H. P., Bradshaw, A. M., Ertl, G., Eds.; *Materials Science Monographs* 57, Elsevier: Amsterdam, 1989.
(97) Witte, G. Private communication.
(98) *Adsorption on Ordered Surfaces of Ionic Solids and Thin Films*; Freund, H. J., Umbach, E., Eds.; Springer-Verlag: Berlin, 1993.
(99) Glebov, A.; Toennies, J. P.; Weiss, H. *Surf. Sci.* **1996**, *351*, 200.
(100) Witte, G.; Wöll, Ch. *J. Chem. Phys.* **1995**, *103*, 5860.
(101) Chesters, M. A.; Gardner, P.; McCash, E. M. *Surf. Sci.* **1989**, *209*, 89. Firment, L. E.; Samorjai, G. A. *J. Chem. Phys.* **1993**, *69*, 3940. Raval, R.; Parker, S. F.; Chesters, M. A. *Surf. Sci.* **1993,** *289*, 227. Dudde, R.; Reihl, B. *Chem. Phys. Lett.* **1992**, *196*, 91.
(102) Celli, V.; Eichenauer, D.; Kaufold, A.; Toennies, J. P. *J. Chem. Phys.* **1985**, *83*, 2504.
(103) See for example: Lennard-Jones, J. E.; Dent, B. M. *Trans. Faraday Soc.* **1928**, *24*, 92. Gevirzman, R.; Kozirovski, Y.; Folman, M. *Trans. Faraday Soc.* **1969**, *65*, 2206. Heidberg, J.; Singh, R. D.; Chen, C. F. *Z. Phys. Chem. N. F.* **1978**, *110*, 135. Polanyi, J. C.; Williams, R. J.; O'Shea, S. F. *J. Chem. Phys.* **1991**, *94*, 978.
(104) Heidberg, J.; Kampshoff, E.; Kühnemuth, R.; Schönekäs, O. *Surf. Sci.* **1991**, *251/252*, 314. The numbers quoted in the text are based on later refinements of the potential as described in ref 108.
(105) Schimmelpfennig, J.; Fölsch, S.; Henzler, M. *Surf. Sci.* **1991**, *250*, 198.
(106) Heidberg, J.; Kampshoff, E.; Kühnemuth, R.; Schönekäs, O. *Surf. Sci.* **1992**, *269/270*, 120.
(107) Liu, G.-Y.; Robinson, G. N.; Scoles, G.; Heiney, P. A. *Surf. Sci.* **1992**, *262*, 409. A reinterpretation of the $(2\sqrt{2} \times 2\sqrt{2})$R45° pattern is discussed in ref 108.
(108) Lange, G.; Schmicker, D.; Toennies, J. P.; Vollmer, R.; Weiss, H. *J. Chem. Phys.* **1995**, *103*, 2308.
(109) Heidberg, J.; Kampshoff, E.; Künemuth, R.; Schönekäs, O.; Lange, G.; Schmicker, D.; Toennies, J. P.; Vollmer, R.; Weiss, H. *J. Electron Spectrosc. Relat. Phenom.* **1993**, *64/65*, 803.
(110) Prince, K. C. *J. Electron Spectrosc. Relat. Phenom.* **1987**, *42*, 217.
(111) Picaud, S.; Hoang, P. N. M.; Girardet, C. *Surf. Sci.* **1995**, *322*, 381.
(112) Bertino, M.; Graham, A.; Hofmann, F.; Silvestri, W.; Toennies, J. P. To be published.
(113) Schachtschneider, J. H.; Snyder, R. G. *Spectrochim. Acta* **1963**, *19*, 117.
(114) Witte, G.; Toennies, J. P. To be published.
(115) Nyberg, C.; Tengstål, C. G.; Andersson, S.; Holmes, M. W. *Chem. Phys. Lett.* **1982**, *87*, 87.
(116) Hofmann, F.; Svenson, U.; Toennies, J. P. To be published.
(117) Meyer, G.; Neu, B.; Rieder, K. H. *Chem. Phys. Lett.* **1995**, *240*, 379.
(118) Braun, J.; Graham, A.; Hofmann, F.; Silvestri, W.; Toennies, J. P.; Witte, G. *J. Chem. Phys.*, submitted for publication.
(119) Voigtländer, B.; Bruchmann, D.; Lehwald, S.; Ibach, H. *Surf. Sci.* **1990**, *225*, 151.
(120) Ha, J. S.; Sibener, S. *Surf. Sci.* **1991**, *256*, 281.
(121) Jones, L. H. *J. Mol. Spetrosc.* **1960**, *5*, 133.
(122) Braun, J.; Kostov, K.; Witte, G.; Wöll, Ch. To be published.
(123) Truong, C. M.; Rodriguez, J. A.; Goodman, D. W. *Surf. Sci. Lett.* **1992**, *271*, L385.
(124) Poelsma, B.; Palmer, R. L.; Comsa, G. *Surf. Sci.* **1984**, *136*, 1.

(125) Hofmann, F. Unpublished results.
(126) Witte, G. Unpublished results.
(127) Pfnür, H.; Feulner, P.; Menzel, D. *J. Chem. Phys.* **1983**, *79*, 4613.
(128) Berndt, R.; Toennies, J. P.; Wöll, Ch. *J. Electron Spectrosc. Relat. Phenom.* **1987**, *44*, 183.
(129) Andersson, S. *Solid State Commun.* **1977**, *21*, 75.
(130) Bertino, M. Unpublished results.
(131) Steininger, H.; Lehwald, S.; Ibach, H. *Surf. Sci.* **1982**, *123*, 264.
(132) Range, H. Unpublished results.
(133) Kisters, G.; Chen, J. G.; Lehwald, S.; Ibach, H. *Surf. Sci.* **1991**, *245*, 65.
(134) Lock, A.; Madden, Witte, G. Unpublished results.
(135) Toennies, J. P.; Wöll, Ch. L.; Zhang, C. *J. Chem. Phys.* **1992**, *96*, 4023.
(136) Lüdecke, J. Unpublished results.
(137) Witte, G.; Braun, J.; Toennies, J. P. To be published.
(138) Kao, C. T.; Blackmann, B. S.; van Hove, M. A.; Somorjai, G. A.; Chan, C. M. *Surf. Sci.* **1989**, *224*, 77.
(139) Singh, J.; Waller, W. K.; Atrei, A.; King, D. A. *Chem. Phys. Lett.* **1991**, *185*, 426.
(140) Bertino, M.; Hofmann, F.; Steinhögl, W.; Witte, G.; Toennies, J. P.; Wöll, Ch. *Appl. Surf. Sci.*, submitted for publication.
(141) Witte, G.; Range, H.; Toennies, J. P.; Wöll, Ch. *Phys. Rev. Lett.***1993**, *71*, 1063.
(142) Keol, B. E.; Crowell, J. E.; Mate, C. M.; Somorjai, G. A. *J. Phys. Chem.* **1984**, *88*, 1988. Mate, C. M.; Somorjai, G. A. *Surf. Sci.* **1985**, *160*, 542.
(143) Bruch, L. W.; Glebov, A.; Toennies, J. P.; Weiss, H. *J. Chem. Phys.* **1995**, *103*, 5109.
(144) Ferry, D.; Gle, A.; Seuz, V.; Suzanne, J.; Toennies, J. P.; Weiss, H. *J. Chem. Phys.*, in press.
(145) Glebov, A.; Toennies, J. P.; Weiss, H. To be published.
(146) Lange, G.; Toennies, J. P.; Weiss, H. To be published.
(147) Gerlach, R.; Glebow, A.; Lange, G.; Toennies, J. P.; Weiss, H. *Surf. Sci.* **1995,** *331−333*, 1490.
(148) Gerlach, R.; Toennies, J. P.; Weiss, H. To be published.
(149) Glebov, A.; Miller, R. E.; Toennies, J. P. To be published.
(150) Gibson, K. D.; Sibener, S. J.; Hall, B. M.; Mills, D. L.; Black, J. E. *J. Chem. Phys.* **1985**, *83*, 4256.
(151) Bertino, M.; Graham, A.; Hofmann, F.; Toennies, J. P.; Wöll, Ch. To be published.
(152) Toennies, J. P.; Vollmer, R. *Phys. Rev. B* **1989**, *40*, 3495.
(153) Rudolf, P.; Astaldi, C.; Cautero, G.; Modesti, S. *Surf. Sci.* **1991**, *251/252*, 127.
(154) Astaldi, C.; Rudolf, P.; Modesti, S. *Solid State Commun.* **1990**, *75*, 847.
(155) Rahman, T. S.; Rocca, M.; Lehwald, S.; Ibach, H. *J. Electron Spectrosc. Relat. Phenom.* **1986**, *38*, 45.
(156) Andersson, S. *Chem. Phys. Lett.* **1978**, *55*, 185.
(157) Taub, H.; Carneiro, K.; Kjems, J. K.; Passell, L.; McTague, J. P. *Phys. Rev. B* **1977,** *16*, 4551
(158) Vollmer, R.; Toennies, J. P. *Phys. Rev. B* **1991**, *44*, 9833.
(159) Schmicker, D.; Toennies, J. P.; Vollmer, R.; Weiss, H. *J. Chem. Phys.* **1991**, *95*, 9412.
(160) DeKieviet, M, Dubbers, D, Schmidt, C, Scholz, D, Spinola, U. *Phys. Rev. Lett.* **1995**, *75*, 1919.
(161) Schief, H.; Marsico, V.; Kuhnke, K.; Kern, K. Submitted for publication.

CR9502209